

Large-Scale Microfluidic Device Fabrication for Non-Equilibrium RNA Kinetic Experiments

CNF Project Number: 692-98

Principal Investigator(s): Lois Pollack

User(s): Alex Plumridge

Affiliation(s): Applied and Engineering Physics, Cornell University

Primary Source(s) of Research Funding: National Institutes of Health

Contact: lp26@cornell.edu, ap866@cornell.edu

Website: <https://pollack.research.engineering.cornell.edu/>

Primary CNF Tools Used: Plasma-Therm deep silicon etcher, substrate bonder, dicing saw, ABM contract aligner, Heidelberg mask writer

Abstract:

Here we report the design and implementation of a large-scale fabrication protocol to produce ~ 100 microfluidic mixing devices per wafer. These devices enable non-equilibrium single-molecule fluorescence measurements. This upgraded protocol improves on our previous work by increasing the yield, number and robustness of devices while decreasing the fluorescence background. Such improvements allow kinetic measurements on RNA to be made more routinely, easily and with higher data quality.

Summary of Research:

Non-equilibrium measurements are powerful tools that can be applied to study biological interactions [1]. The rapid initiation of biological reactions and examination of their time evolution, exposes information that is hidden in simple equilibrium experiments. This technique provides details on short lived intermediates, folding pathways and transition states.

While the benefits of non-equilibrium measurements are numerous, such techniques are rarely applied when compared to their equilibrium counterparts. The major bottle-neck is the lack of commercially available systems to perform these experiments. Only the stopped-flow technique is widely used, but requires high sample volumes, limiting the number of kinetic measurements that have been made. Additionally, in cases where kinetic measurements are applied, the experiments report bulk averages. Therefore, sparse or short-lived intermediates are challenging to identify, and careful analysis is required to resolve the presence of other intermediate states along reaction pathways [2].

Coupling microfluidic mixing to single-molecule fluorescence circumvents the above challenges. Examination of single molecules allows resolution of individual subpopulations within a sample, nanomolar concentrations are used, and ~ms timescales are

accessible using microfluidics, with sparse sample consumption [3]. We previously designed and fabricated microfluidic mixing devices using SU-8 and glass, however this protocol had some disadvantages. The number of devices per wafer was limited by the use of standard sized glass coverslips, and device robustness and fluorescence background were compromised due to the use of an SU-8 sealing layer.

To bypass these limitations, we developed a fabrication protocol where channels are etched into silicon. Full wafers are subsequently anodically bonded to full sized glass wafers to seal devices. The protocol is schematically shown in Figure 1.

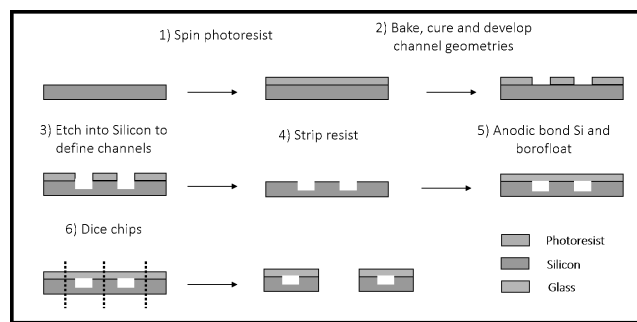


Figure 1: Fabrication process utilized to obtain a large number of robust microfluidic mixing devices.

In brief, a 4 μm thick layer of Shipley resist is spun, baked, and cured on a standard sized silicon wafer. Channel patterns are exposed, and the resist developed. The microfluidic channels are then etched into the silicon using the Plasma-Therm deep silicon etcher — we aim for channel depths of 105 μm . After etching, the resist is removed. The etched silicon piece and a 170 μm thick, full wafer sized borofloat wafer are Piranha cleaned before anodic bonding using the substrate bonder. As a final step, the dicing saw separates individual devices, and liberates channel cross-sections at the edges of each device. Interfacing to the devices is complete by gluing 105 μm outer diameter glass capillary lines into the revealed sockets with UV curable epoxy.

A full wafer of separated devices is shown in Figure 2. Ninety-six devices are made in the same process. On the right, a stereoscope image of a single device from this wafer is shown.

In the stereoscope image, the sockets that interface with external lines are clearly visible. The thin glass layer on top of the silicon base layer is also resolved. Fabrication of devices without an extra adhesive layer in between glass and channel geometries grants higher pressure resilience (as we limit crack propagation at the sealing layer) and reduces the intrinsic fluorescence background from SU-8 and similar epoxies.

Conclusions and Future Steps:

Here we describe an improved fabrication protocol that yields silicon microfluidic mixers as opposed to recent

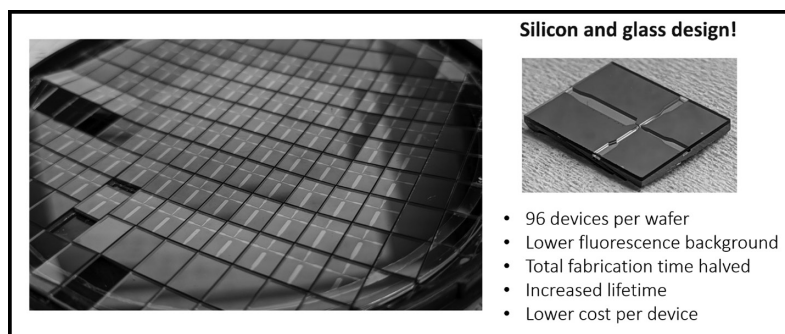


Figure 2: The left shows a wafer of microfluidic devices after the final dicing step. On the right is a stereoscope image of a single device. The thin glass layer can be seen covering the base silicon wafer. Sockets liberated during dicing process are present at the end of the channel and facilitate the connection of fluid lines using UV curable epoxy.

- Silicon and glass design!**
- 96 devices per wafer
 - Lower fluorescence background
 - Total fabrication time halved
 - Increased lifetime
 - Lower cost per device

past efforts using glass and SU-8. This new protocol creates many more devices per wafer, at lower cost and reduced fabrication time per piece. We are now positioned to pursue non-equilibrium RNA folding experiments without concern for device robustness, lifetime or inventory.

References:

- [1] Al-Hashimi, H. M.; Walter, N. G. *Curr. Opin. Struct. Biol.* 2008, 18 (3), 321.
- [2] Daniels, K. G.; Suo, Y.; Oas, T. G. *Proc. Natl. Acad. Sci.* 2015, 112 (30), 9352.
- [3] Wunderlich, B.; Nettels, D.; Benke, S.; Clark, J.; Weidner, S.; Hofmann, H.; Pfeil, S. H.; Schuler, B. *Nat. Protoc.* 2013, 8 (8).

Body-on-a-Chip Systems for Studying Liver Metastasis

CNF Project Number: 731-98

Principal Investigator(s): Michael L. Shuler, Harold G. Craighead

User(s): Ying Wang, Paula Miller, Vivek Sitaram Jadhav

Affiliation(s): Nancy E. and Peter C. Meinig School of Biomedical Engineering, Robert Frederick Smith School of Chemical and Biomolecular Engineering; Cornell University

Primary Source(s) of Research Funding: National Center for Advancing Translational Sciences, National Science Foundation, National Institutes of Health

Contact: mls50@cornell.edu, hgc1@cornell.edu, ying.wang@cornell.edu, pgm6@cornell.edu, vj76@cornell.edu

Primary CNF Tools Used: VersaLaser engraver/cutter tool, ABM contact aligner, SU-8 hot plates, SUEX/ADEX laminator, PDMS casting station, hot press, Objet30 Pro 3D printer

Abstract:

Our organ-on-a-chip devices are physiological tissue-engineered microsystems that mimic human organs, structurally and functionally [1]. Human cell-based multi-organ on-a-chip systems, could be used for drug development [2], simulate human physiology and disease progression. The organ-organ interactions offer more accurate predictions of human responses to therapeutics and provide mechanistic insights into human diseases, while significantly reduce drug development cost and animal usage. Currently, we are developing several microphysiological systems, which are fabricated with tools at CNF, and will be used to study chemotherapeutic toxicity, model cancer cell metastasis, and simulate immune responses.

Summary of Research:

Here, we describe two unidirectional metastatic devices to study colon cancer metastasis and the human liver sinusoidal vasculature for colon cancer extravasation. The both devices have unidirectional flow; colon-liver chip is “pumpless” using a rocker platform for fluid (blood surrogate) unidirectional recirculation and the liver sinusoidal vascular chip is a gravity-driven single pass microfluidic platform.

Colon-Liver Chip:

We have modified our original dual-organ-on-a-chip system to model colorectal cancer (CRC) liver metastasis. This microphysiological system is based on a pumpless platform [3,4]. Two organ chambers representing colon and liver are interconnected and perfused with gravity-driven flow at physiological perfusion rates [5]. The frame was milled out of a polycarbonate sheet with silicone gaskets to help seal the device. Microfluidic channels, chambers and medium reservoirs were patterned with laser ablation into a poly(methyl methacrylate) (PMMA) sheet and/or silicone sheets using the VersaLaser VLS3.60 Cutting and Engraving CO₂ Laser (Universal Laser Systems, Scottsdale, Arizona) at CNF. The flow

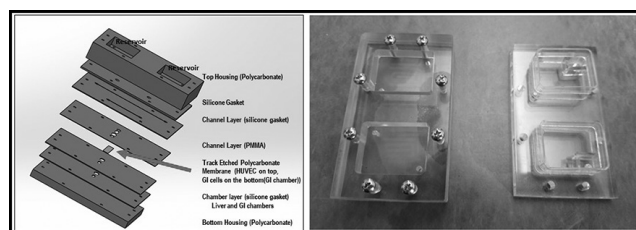


Figure 1: Design of the two-chamber unidirectional device for liver metastasis. Schematic view and actual photographs of the assembled frames.

dynamics were characterized computationally and experimentally. Flow rates were measured to be within 15% of the designed values. The prototype devices tested with colon and liver cells maintained greater than 85% cell viability.

Using this colon-liver platform, we will incorporate organotypic CRC model and 3D liver constructs to investigate the metabolic stress due to CRC liver metastasis. We will investigate the cellular interaction, differentiation, migration and invasion of primary tumor and metastatic fibroblast tumor microenvironment to evaluate contributing factors in CRC metastasis [Fig.1].

Liver Sinusoidal Vascular Chip:

We have designed and constructed a gravity-driven microfluidic platform for modeling the human liver sinusoidal microenvironment and investigating the extravasation of liver metastatic colorectal cancer (CRC) cells. The frame was fabricated in poly(methyl methacrylate) (PMMA). PMMA layers of desired thickness were patterned using a CO₂ laser (VersaLaser VLS3.50), and were bond together using a hot press at CNF after a 15 min UV/Ozone (Samco UV and Ozone stripper) exposure. Also, flow-through microfluidic channels and chambers were patterned with laser ablation into silicone sheets using the VersaLaser. A propeller stirring device was designed in Inventor to overcome the issue of settling, attachment and aggregation of CRC cells in the feed reservoirs. The propeller stirring device was fabricated using the Objet30 Pro 3D printer at CNF.

The stirring device was driven by a small stir bar on a magnetic stirrer. We have tested different propeller designs, the positioning in the reservoir, and the stirring speed, to optimize stirring scheme that produced minimal cell aggregation while preserving maximal cell viability. We are currently focusing on characterizing the phenotype of liver sinusoidal endothelial cells in our microfluidic model and comparing CRC cell interactions with human liver sinusoidal endothelial cells versus human umbilical vascular endothelial cells [Figure 2].

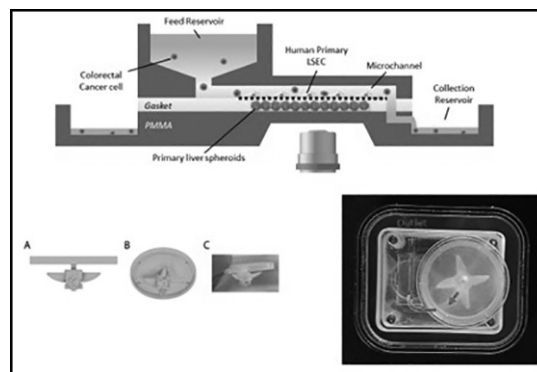


Figure 2: Design of the human liver sinusoidal vasculature for colon cancer extravasation. Schematic views of the device and the propeller stirring device with actual photographs.

References:

- [1] Wang YI, Carmona C, Hickman JJ, Shuler ML. Multiorgan Microphysiological Systems for Drug Development: Strategies, Advances, and Challenges. *Adv Healthc Mater*;7:1701000. doi.org/10.1002/adhm.201701000.2 (2018).
- [2] Sung JH, Wang YI, Narasimhan Sriram N, Jackson M, Long C, Hickman JJ, et al. Recent Advances in Body-on-a-Chip Systems. *Anal Chem*;91:330-51. doi.org/10.1021/acs.analchem.8b05293.3 (2019).
- [3] Price PS, Conolly RB, Chaisson CF, Gross E a, Young JS, Mathis ET, Tedder DR. Modeling interindividual variation in physiological factors used in PBPK models of humans. *Crit Rev Toxicol*;33(5):469-503. doi:10.1080/713608360 (2003).
- [4] Brown RP, Delp MD, Lindstedt SL, Rhomberg LR, Beliles RP. Physiological Parameter Values for Physiologically Based Pharmacokinetic Models. *Toxicol Ind Health*;13(4):407-484. doi:10.1177/074823379701300401 (1997).
- [5] Forrester DW, Spence VA, Walker WF. The measurement of colonic mucosal, submucosal blood flow in man. *J Physiol*;299(1):1-11. doi:10.1113/jphysiol.1980.sp013106 (1980).

Mechanical Unzipping of DNA Molecules in Parallel Using Nanophotonic Tweezers

CNF Project Number: 1738-08

Principal Investigator(s): Michelle D. Wang

User(s): Fan Ye, Yifeng Hong

Affiliation(s): a) Department of Physics, Cornell University; b) Howard Hughes Medical Institute

Primary Source(s) of Research Funding: Howard Hughes Medical Institute

Contact: mdw17@cornell.edu, fy72@cornell.edu, yh874@cornell.edu

Website: <http://wanglab.lassp.cornell.edu/>

Primary CNF Tools Used: ASML deep ultraviolet stepper, Oxford 100 plasma etcher, Unaxis 770 deep Si etcher, Heidelberg mask writer DWL2000, SÜSS MA6-BA6 contact aligner, Gamma automatic coat-develop tool, LPCVD nitride - B4 furnace, wet/dry oxide - B2 furnace, N2 annealing - B1 furnace, AJA sputter deposition, CVC sputter deposition, GSI PECVD, Oxford PECVD, SC4500 odd-hour evaporator, Zeiss Supra SEM, Zeiss Ultra SEM

Abstract:

Optical trapping has become a major technique widely used in biological and materials sciences, on size scales ranging from the single molecule to the cellular level, and force scales ranging from sub piconewton (pN) to tens of pN [1]. The rapid development of nanofabrication techniques in the past few decades has bolstered the emergence of nanophotonic evanescent-field traps. The ability of nanostructures to direct and confine light beyond the diffraction limit enables miniaturized, on-chip devices with abilities beyond traditional microscope-based optical tweezers [2,3]. The Wang lab has developed and implemented such an on-chip device based on Si or Si₃N₄ waveguides, coined a nanophotonic standing-wave array trap (nSWAT), that allows for controlled and precise manipulation of trapped single biomolecule (such as DNA) arrays via microparticle handles [4-7]. We present here the latest development of the nSWAT platform based on a resonator design that achieves large enough manipulation forces for mechanical unzipping an array of DNA molecules. This benchmark achievement is one step closer to the full realization of nanophotonic tweezers' capabilities, promising increased accessibility and expansion of these platforms to a wide range of biological and biomedical research topics.

Summary of Research:

Over the past decade, the Wang lab has demonstrated a high-throughput, near-field nanophotonic trapping platform that achieves stable trapping and precision manipulation of microparticles [4-7]. The kernel of this platform is the formation of standing waves along a nanophotonic waveguide: by counter propagating two coherent laser beams along a single mode nanophotonic waveguide. The antinodes of the standing wave form an array of stable optical traps. We call this type of trap a nanophotonic standing-wave array trap (nSWAT). By tuning the phase difference between the two counter-propagating laser beams via thermo-optic effect, the antinode locations can be precisely repositioned, and consequently, the optical trap positions can be precisely manipulated. The nSWAT platform holds the capability for high throughput precision measurements for single biomolecules.

Since 2018, we have implemented major upgrades of the nSWAT platform, including the following three aspects.

(1) We have implemented a resonator-based design for ultimate local intensity enhancement into the nSWAT devices. Compared to previous designs, this resonator design gives the highest force enhancement factor, limited only by the total scattering loss of the trapped beads onto the waveguide. We have measured around four times force enhancement, reaching > 30 pN, significantly larger than our previous force-double design [6].

(2) We have implemented a balanced layout and differential operation mode for the micro heaters. This greatly reduced the response time of the micro heaters (from ~ 30 μs to ~ 1 μs). This is shown to be crucial

for maintaining high trapping forces for a trapped bead under strong biased forces under single molecule manipulations.

(3) We have also designed a special sample holder for the nSWAT chip that can greatly reduce (by two orders of magnitude) the thermal drift of the sample caused by the micro heaters. This greatly enhanced the thermal stability of the nSWAT devices. Thanks to the above described improvements, we have achieved mechanical DNA unzipping on the nSWAT devices for the first time.

In the past year, we have continued optimizing the nSWAT platform to achieve our final goal of unzipping an array of DNA molecules. We have further optimized the flow chamber design of the nSWAT devices to achieve better DNA molecule trapping efficiency. We have also implemented SU-8 layer as the anti-corrosion protection layer for the nSWAT device which works significantly better than the Si_3N_4 protection layer we used before [5]. With all these improvements, we are looking forward to the achievement of trapping and unzipping an array of DNA molecules in the near future. Our development and improvement of the nSWAT platform has led to seven publications in the past few years [2-7], and more to come later this year.

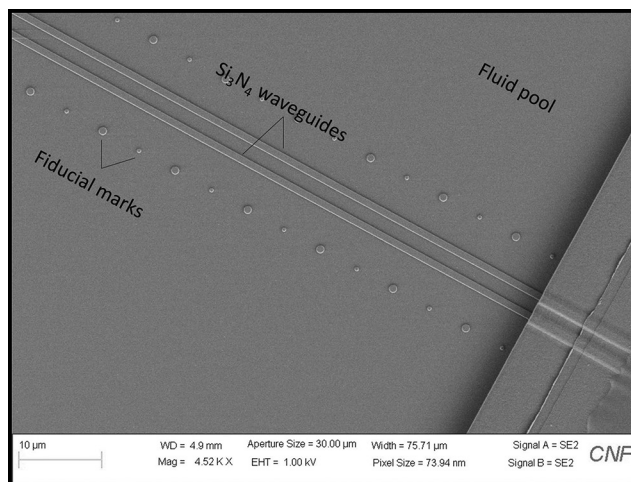


Figure 1: An SEM image of the step boundary of the fluid pool region. Inside the fluid pool region, the two parallel Si_3N_4 waveguides trap two arrays of polystyrene microbeads (380 nm diameter) with DNA molecules tethered in between. The dot arrays near the parallel waveguides are fiducial marks for local position tracking.

References:

- [1] J. L. Killian, F. Ye, M. D. Wang, "Optical Tweezers: A Force to Be Reckoned With" *Cell* 175 (6), 1445-1448 (2018).
- [2] J. E. Baker, R. P. Badman, and M. D. Wang, "Nanophotonic trapping: precise manipulation and measurement of biomolecular arrays" *WIREs Nanomed Nanobiotechnol.* e1477 (2017).
- [3] R. Badman, F. Ye, M.D. Wang, "Towards biological applications of nanophotonic tweezers" *Current Opinion in Chemical Biology* 53, 158-166 (2019).
- [4] M. Soltani, J. Lin, R. A. Forties, J. T. Inman, S. N. Saraf, R. M. Fulbright, M. Lipson, and M. D. Wang, "Nanophotonic trapping for precise manipulation of biomolecular arrays" *Nature Nanotechnology* 9(6), 448-452 (2014).
- [5] F. Ye, R. P. Badman, J. T. Inman, M. Soltani, J. L. Killian, and M. D. Wang, "Biocompatible and high stiffness nanophotonic trap array for precise and versatile manipulation" *Nano Letters* 16(10), 6661-6667 (2016).
- [6] F. Ye, M. Soltani, J. T. Inman, and M. D. Wang, "Tunable nanophotonic array traps with enhanced force and stability" *Optics Express* 25 (7) 7907-7918 (2017).
- [7] R. Badman, F. Ye, W. Caravan, and M. D. Wang, "High Trap Stiffness Microcylinders for Nanophotonic Trapping" *ACS Appl. Mater. Interfaces* 11 (28), 25074-25080 (2019).

Bacterial Mechanics and Mechanobiology

CNF Project Number: 1970-10

Principal Investigator(s): Christopher J. Hernandez

User(s): Christine E. Harper, Melanie F. Roberts, Junsung Lee

*Affiliation(s): Sibley School of Mechanical and Aerospace Engineering,
Meinig School of Biomedical Engineering, Cornell University*

Primary Source(s) of Research Funding: Army Research Office Grant Number W911NF-19-1-0121

Contact: cjh275@cornell.edu, ce272@cornell.edu, mfr75@cornell.edu, jl3939@cornell.edu

Website: hernandezresearch.com

Primary CNF Tools Used: ASML, Oxford 100, AJA sputter deposition, VersaLaser, MOS clean anneal

Abstract:

Bacteria naturally experience mechanical forces in the environment. Mechanical stresses and strains are generated as bacteria swim in fluids, attach to surfaces, grow in biofilms, and even during normal internal pressure homeostasis. Recent studies have shown that bacteria can sense and respond to mechanical forces, and mechanical stress and strain can influence cell division, cell shape, virulence, biofilm initiation, motility, and toxin resistance. However, because of the small scale of bacteria, it is a challenge to apply controlled mechanical stimuli on a single cell level. We developed a microfluidic platform to apply mechanical loads to single bacteria cells *in vivo*. We used this microfluidic platform as a method of applying mechanical stimuli to *Escherichia coli* (*E. coli*) and determining how mechanical stress affects a group bacterial cell envelope proteins used for toxin and antibiotic resistance. In addition, we are using this microfluidic device in the first step toward determining the mechanical properties of the bacterial cell envelope.

Summary of Research:

Our work involves the use of microfluidic devices as tools for mechanical testing of live bacteria. Within our devices, individual bacteria are flowed into tapered channels and trapped (Figure 1). The bacteria experience mechanical loading from the hydrostatic fluid pressure as well as contact with the tapered channels walls (Figure 2). Key advantages of this microfluidic platform include minimal sample preparation, no chemical immobilization or labeling, the ability to analyze hundreds of cells at once, and the ability to apply different magnitudes of mechanical loading to different bacteria simultaneously [1]. We manufactured devices on silica glass wafers using deep UV photolithography to achieve nanoscale features (250 nm smallest dimension). These glass-on-glass devices were manufactured using the ASML, Oxford 100, AJA sputter deposition, VersaLaser, and MOS clean anneal tools at the Cornell NanoScale Science and Technology Facility.

Recently we have investigated the effects of mechanical stress and strain on the functionality of multicomponent efflux complexes in bacteria. Multicomponent efflux complexes create channels that cross the cell envelope of bacteria and are used to remove toxins including metal ions and antibiotics. Since multicomponent efflux complexes form a rigid link across the cell envelope, we targeted them as being sensitive to changes in cell envelope stress caused by mechanical loading in our microfluidic device. Our data suggests that the assembly and function of the multicomponent efflux

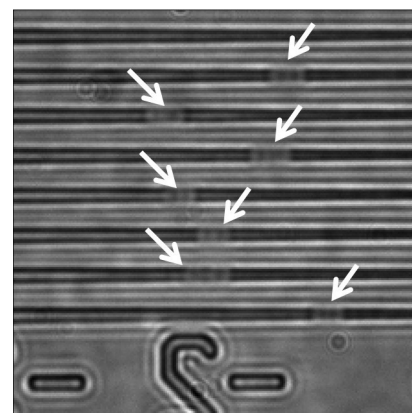


Figure 1: *E. coli* cells trapped within the tapered channels of the microfluidic device. Fluid pressure is used to flow the bacteria into the tapered channels.

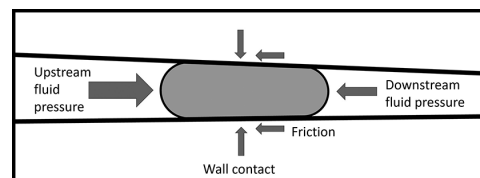


Figure 2: The bacteria cells experiences mechanical loading in the tapered channels due to the hydrostatic pressure, which varies from the upstream end to the downstream end, and due to contact with the walls of the tapered channel.

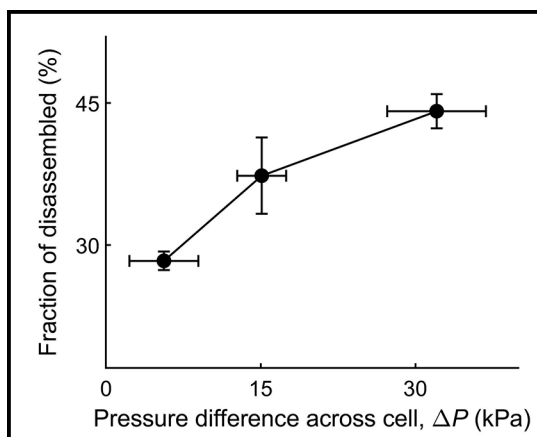


Figure 3: Increased pressure difference across the cell, which correlates with increased applied mechanical load, was shown to increase disassembly of the multicomponent efflux complex CusCBA in *E. coli*.

complex CusCBA in *E. coli* is impaired by increased mechanical stress. Increased applied mechanical stress due to increased pressure in our microfluidic device was shown to promote disassembly of the CusCBA efflux complex (Figure 3). Disassembled CusCBA complexes are nonfunctional and incapable exporting copper ion toxins, suggesting copper ion resistance of mechanically stressed cells is reduced [2]. We are currently investigating if mechanical stress in the cell envelope affects other trans-envelope multicomponent complexes. Preliminary evidence shows that assembly of the multicomponent efflux complex MacABTolC, a multicomponent efflux complex that contributes to macrolide antibiotic resistance, is also sensitive to mechanical stress [3].

Conclusions and Future Steps:

So far, we have seen that in *E. coli* mechanical stress and strain impairs the proper assembly and function of some of the cellular machinery needed for toxin and antibiotic resistance. In the future we will focus on using our microfluidic device to quantify the mechanical properties of the bacterial cell envelope. Establishing a reliable method of measuring the mechanical properties of the bacterial cell envelope will help us identify subcellular components that contribute to bacterial mechanics as well as how different environmental factors such as antibiotic treatment can change bacterial

mechanical properties. Measuring bacterial mechanical properties has historically been quite challenging and has mostly been limited to atomic force microscopy measurements using fixed bacteria, which has limitations due to uncertain boundary conditions and difficulties separating internal pressure from membrane elasticity [4]. We are working to better understand bacterial mechanical properties by combining experimental data from the microfluidic devices with finite element modelling to calculate numerical estimates for the Young's Modulus of the bacterial cell envelope.

References:

- [1] X. Sun, W.H. Weinlandt, H. Patel, M. Wu, C.J. Hernandez. (2014) "A Microfluidic Platform for Profiling Biomechanical Properties of Bacteria." *Lab Chip*. 14 (14), 2491-2498. NIHMS600175.
- [2] L.A. Genova, M.F. Roberts, Y.C. Wong, C.E. Harper, A.G. Santiago, B. Fu, A. Srivastava, W. Jung, L.M Wang, Krzemiski, X. Mao, X. Sun, C.Y. Hui, P. Chen, C.J. Hernandez. (2019) "Mechanical stress compromises multicomponent efflux complexes in bacteria". *Proceedings of the National Academy of Sciences U. S. A.* 116 (51) 25462-25467.
- [3] C.E. Harper, W. Zhang, P. Chen, C.J. Hernandez. (2020) "Mechanical stress promotes disassembly of the antibiotic efflux complex MacAB-TolC". *Biophysical Society Annual Meeting*. San Diego, CA, USA.
- [4] C.E. Harper, C.J. Hernandez. (2020) "Cell biomechanics and mechanobiology in bacteria: Challenges and opportunities". *Applied Physics Letters Bioengineering*. 4 (2) 201501.13

Robotic Microswimmers Powered by Ultrasound for Biomedical Applications

CNF Project Number: 2068-11

Principal Investigator(s): Mingming Wu

User(s): Tao Luo

Affiliation(s): Department of Biological and Environmental Engineering, Cornell University

Primary Source(s) of Research Funding: National Cancer Institute

Contact: MW272@cornell.edu, TL565@cornell.edu

Primary CNF Tools Used: Heidelberg mask writer-DWL2000, ABM contact aligner, scanning electron microscope (SEM)

Abstract:

Microrobotics, an interdisciplinary field that combines robotics, micro/nanotechnology, biomedical engineering, and materials science, paves a novel way for biomedical applications, such as targeted drug and/or cell delivery for cancer therapy. However, the technology itself is still at an infant stage before reaching the full potential for various biomedical applications. In this project, we are aiming to develop an untethered microrobotic swimmer that can be propelled and navigated in liquids using an external ultrasound. A challenging aspect of the project is to develop the nano-size flagellum that can be used to propel the robotic swimmers in fluids. As a first step of this project, we engineered a microcantilever that will be used as the micropropeller for the microswimmer. This SU-8 microcantilever was fabricated using a two-layer photolithography along with a sacrificial layer for releasing.

Summary of Research:

Robotic microswimmers, which have the capability to be propelled and navigated wirelessly in biological fluid, can open new doors for addressing very challenging issues in biomedical fields, such as targeted drug delivery. However, the size of microswimmers, which is usually smaller than one millimeter, made it difficult for on-board integration of components, such as batteries and motors. Hence, novel powering and propulsion mechanisms are demanded. Studies on using various untethered external power sources

showed that magnetic and ultrasonic waves were the most promising candidates for *in vivo* applications. In contrast to magnetic actuation, ultrasonic wave has the advantages of low cost and long distance control. Here, we designed a simple microcantilever for the studies of cantilever fluid interaction, in particular, the fluid streaming behavior when the cantilever is under resonance. This study will lay a foundation for the micro-propeller design in future work.

To fabricate the microcantilever structure, we have developed a modified two-layer SU-8 process along with a sacrificial layer (PVA) release method. First, a two-layer SU-8 structure was fabricated on a PVA coated 4-inch silicon wafer by using the standardized alignment photolithography (Figure 1A). Here, the pattern of the bottom layer consists of the cantilevers and that of the top layer supporting structures for the cantilever. (See Figure 1A).

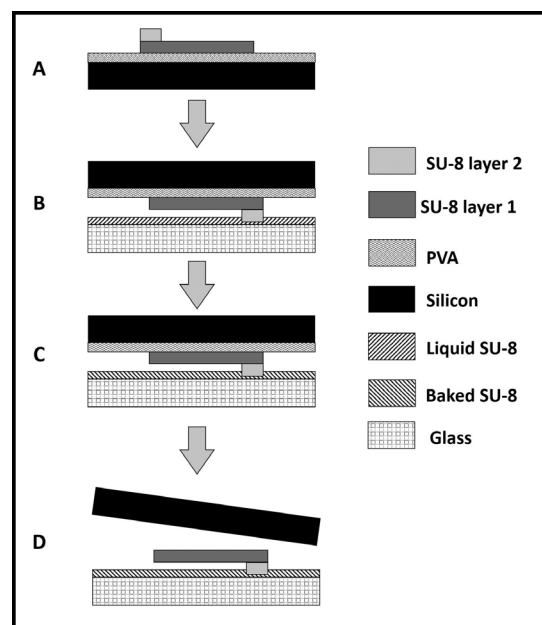


Figure 1: Fabrication process of the SU-8 microcantilever. (A) A two-layer SU-8 structure is fabricated on the PVA coated Si wafer by using alignment photolithography of two SU-8 layers. (B) PVA coated Si wafer with two-layer SU-8 structures is flipped and put on glass slide with a thin layer of liquid SU-8. (C) The sandwiched device is baked to solidify the liquid SU-8 layer on the glass slide. (D) The sandwiched device is immersed into water for 30 min to dissolve the PVA layer and release the Si wafer.

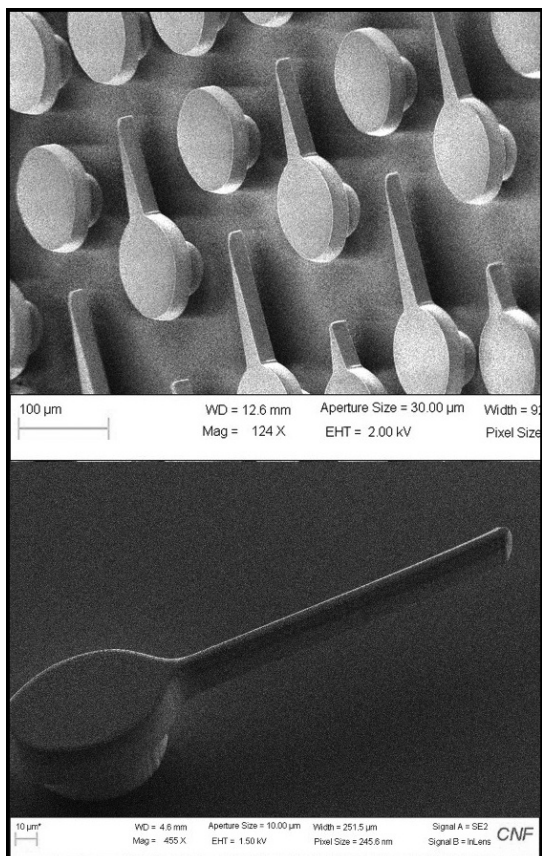


Figure 2: SEMs of SU-8 microcantilevers on glass slides.

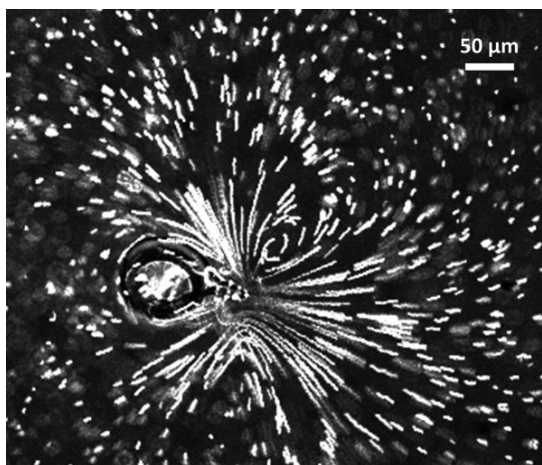


Figure 3: Acoustic streaming of a microcantilever in water revealed by fluorescent microsized beads when the cantilever is excited by the 1.35 MHz ultrasound.

Second, the silicon wafer with the two-layer SU-8 structures was flipped and put on a glass slide, which has been coated with a liquid SU-8 layer (Figure 1B). Then, the sandwiched structure was placed on the hot plate and baked under 95°C for 15 min to solidify the liquid SU-8 layer (Figure 1C). In this way, the second SU-8 layer from the silicon wafer was glued on the glass slide. After cooling down with the hot plate, the sandwiched structure was immersed into water for 30 min to dissolve the PVA layer, and the two-layer SU-8 structure was transferred from the silicon wafer to the glass slide (Figure 1D). In this way, the first and second layer of SU-8 on the silicon wafer has been flipped on the glass slide, which formed a cantilever structure.

The quality of the fabricated microcantilevers can be very good, even for structures with high aspect ratios (Figure 2).

The fabricated microcantilevers were immersed into the water, and an ultrasonic transducer was used to transmit ultrasound waves in the water to excite the microcantilevers. We have tuned the frequency of the ultrasound waves to detect the resonance frequency of the microcantilever based on the magnitude and pattern of the streaming flow around the microcantilever. A dual vortex like flow pattern was visualized by putting 0.83 µm fluorescent polystyrene microbeads when the microcantilever was excited under its first resonance (Figure 3).

Conclusions and Future Steps:

In this work, we fabricated SU-8 microcantilevers by integrating a two-layer SU-8 photolithography method with a PVA sacrificial releasing method. The microcantilever was used as the simplest model for understanding the fluid-structure interaction under ultrasonic excitation. We had successfully excited the fabricated microcantilever remotely by using ultrasound and observed the streaming flow for the first vibration mode of the microcantilever. Future study will be quantitatively characterizing the propulsion force generated by streaming flows under different excitation conditions.

Microfabrication of Fixed Length Sample Holders for Cryogenic Small Angle X-Ray Scattering

CNF Project Number: 2157-12

Principal Investigator(s): Robert Thorne

User(s): David Moreau

Affiliation(s): Cornell Laboratory of Atomic and Solid State Physics, Cornell University

Primary Source(s) of Research Funding: National Institutes of Health

Contact: ret6@cornell.edu, dwm265@cornell.edu

Primary CNF Tools Used: Heidelberg mask writer - DWL2000, SÜSS MA6-BA6 contact aligner, Oxford 80, Objet30 Pro 3D printer, VersaLaser engraver/cutter tool, YES polyimide curing oven, potassium hydroxide wet etch station

Abstract:

Small-angle X-ray scattering (SAXS) is a key tool for probing the structure and function of proteins, nucleic acids, and macromolecular complexes. Most synchrotron sources have dedicated BioSAXS beam lines, but efforts to improve their throughput have not kept pace with user demand. Large sample volumes and low duty cycles are critical bottlenecks in the expansion of BioSAXS. Cryogenic sample freezing overcame these bottlenecks in an analogous X-ray technique, macromolecular crystallography. Cryocooling significantly reduces the effects of X-ray radiation damage, reducing the necessary sample volume to collect adequate amounts of data, and eases the sample handling of sensitive or unstable samples. Likewise, CryoSAXS should require much smaller sample volumes per measurement, allow sample preparation in the home lab immediately after purification, easy sample storage and shipping, and automated high-throughput data collection. This will enable dramatically more efficient use of both biomolecules and synchrotron beam time, and significantly expand the potential scope of BioSAXS studies.

Summary of Research:

We envision CryoSAXS as a routine method analogous to cryocooling in macromolecular crystallography (MX). The reduction in radiation damage at $T = 100$ K significantly reduces the amount of protein required per measurement and sample holders compatible with standard macromolecular cryocrystallography (MX) infrastructure could be transformative step in increasing the throughput and potential of BioSAXS. CryoSAXS could be especially useful for high-throughput parameter and ligand interaction screening and for study of difficult to produce proteins or complexes, applications in which BioSAXS may have the greatest impact on human health.

Despite the demonstrations of its potential [1,2], the lack of a robust experimental platform has prevented CryoSAXS from becoming a routine experimental technique. The need to subtract a highly matched background scattering pattern from the macromolecule's scatter and the difficulty in vitrifying bulk-like solutions have posed serious technical challenges for the development of sample holders adequate for routine use. Shown in Figure 1 is a new generation of CryoSAXS devices we recently developed using microfabrication techniques at the Cornell NanoScale Science and Technology Facility (CNF).

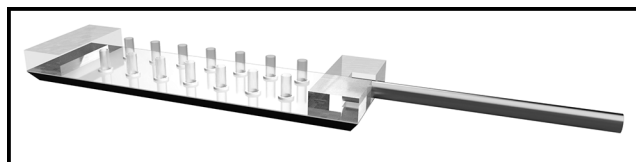


Figure 1: Computer generated image of CryoSAXS sample devices. The sample is held in place between two silicon nitride X-ray windows by Kapton tube. The X-ray passes axially through the tubing. Multiple sample cells are present in a single device in two rows. One row contains solutions with a macromolecule and the other is analogous solutions without the macromolecule to be used for background subtraction.

These devices constrain the sample held between two silicon nitride windows at a 1 mm fixed pathlength. Double-sided polished wafers coated in 500 nm of low-pressure chemical vapor deposited silicon nitride were procured from Silicon Valley Microelectronics. One side of the wafer was patterned with photoresist then dry etched to remove the nitride for a later potassium hydroxide (KOH) wet etch. SU-8 was deposited and patterned on the other side to serve as a hydrophobic layer to aid in the pinning of the sample to the X-ray windows. A KOH wet etch then formed the X-ray windows and diced the wafer. Spacers were laser cut

from 1 mm thick quartz glass sheets then glued to one portion of the wafer pieces. Using laser cut jigs, 1 mm long Kapton tubing was cut and glued to the devices. The devices are filled from the open end of the tube, then a second wafer piece is affixed to the top of the device to seal the sample. The samples are then cryogenically frozen by plunging into liquid nitrogen (LN_2), stored in LN_2 and later mounted in an X-ray beam while being kept at $T = 100$ K by a cold gas stream.

X-ray data collection was performed at Cornell High Energy Synchrotron Source (CHESS) beamline ID7A1 for the protein apoferritin using 45% w/w propylene glycol as a cryoprotectant. Figure 2 shows results from apoferritin at three different protein concentrations. Figure 2a shows the background subtracted X-ray diffraction intensity. The inset shows this data in a Guinier plot. Deviations from linearity at low scattering angles are indicative poor data quality, including incorrect background subtraction at low scattering angles. The normalized Kratky plot in Figure 2b. This should go to zero at higher scattering angles for globular proteins such as apoferritin. Deviations indicate incorrect background subtraction at high scattering angles.

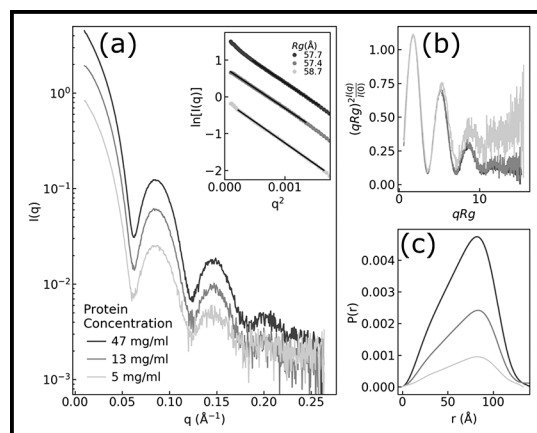


Figure 2: Background subtracted X-ray diffraction intensity from apoferritin at three different concentrations.

Conclusions and Future Steps:

The development and subsequent adoption of cryogenic methods for BioSAXS could significantly increase sample throughput and reduce sample consumption, enabling SAXS to extend to a larger user base. It could open up the possibility of new science through high-throughput screening of ligands or other therapeutics. CryoSAXS's potential has been known for a while, but critical technical challenges have prevented the widespread adoption of the method. A well-matched background for subtraction is necessary for SAXS and the cryocooling step tends to introduce significant variability to the background. X-ray scatter from ice present in the sample quickly overwhelms the scatter from the protein, as does parasitic scatter from a sample that has cracked under the stress induced by cryocooling. This new generation of devices is designed to maximize the sample's cooling rates and minimize internal stress. Future steps involve the refinement of this technique through iterative design.

References:

- [1] Meisburger, S. P., et al., (2013) *Biophys. J.*, 104, 227-236.
- [2] Hopkins, J. B., et al., (2015) *J. Appl. Cryst.* 48, 227-237.

Dual-Gradient Microhabitat Platform for Microalgae Growth

CNF Project Number: 2262-13

Principal Investigator(s): Dr. Mingming Wu

User(s): Fangchen Liu

Affiliation(s): Department of Biological and Environmental Engineering, Cornell University

*Primary Source(s) of Research Funding: United State Department of Agriculture -
National Institute of Food and Agriculture*

Contact: MM272@cornell.edu, FL373@cornell.edu

Website: biofluidics.bee.cornell.edu

Primary CNF Tools Used: Heidelberg mask writer - DWL2000, ABM contact aligner, P10 profilometer, MVD 100

Abstract:

The occurrence of harmful algal blooms (HABs) is increasing at an alarming rate worldwide, threatening water resources and aquatic ecosystems. Nutrients are known to trigger the onset of HABs and systematic investigation at a cellular level is lacking. To study the combination effects of multiple nutrients on microalgae growth in a high throughput way, a dual-gradient microhabitat platform was designed, fabricated, and characterized. Using the platform, the synergistic effect of nitrogen and phosphorous on the growth of model microalgal *Chlamydomonas reinhardtii* was revealed.

Summary of Research:

Harmful algal blooms, or HABs, are serious environmental problems, where a sudden growth of algae or cyanobacteria poses a threat to freshwater and marine ecosystems. HABs deteriorate drinking water quality and have huge environmental and economical costs. Nutrient enrichment is believed to be the fundamental cause of HABs, and climate change may further intensity the problem [1]. However, there lacks a quantitative/mechanistic understanding of the roles of environmental factors in the onset of HABs at a cellular level. The goal of this project is to investigate the synergistic roles of multiple environmental factors in the growth of cyanobacteria.

Environmental conditions known to affect algae growth include nutrients, mainly nitrogen (N) and phosphorous (P), light intensity and temperature. These conditions are hard to control in nature, and also cannot be quantified in a high throughput way in flasks and chemostats. Previously, a high throughput array microhabitat platform has been developed in our lab that is suitable for monitoring growth of photosynthetic microbes [2], which is capable of generating a stable single nutrient gradient. Using this platform, we discovered that the growth rates of *Chlamydomonas reinhardtii* (*C. reinhardtii*) in the presence of NH_4Cl gradient fit into a modified Monod kinetics model with the half saturation constant of NH_4Cl to be $1.2 \pm 0.3 \mu\text{M}$.

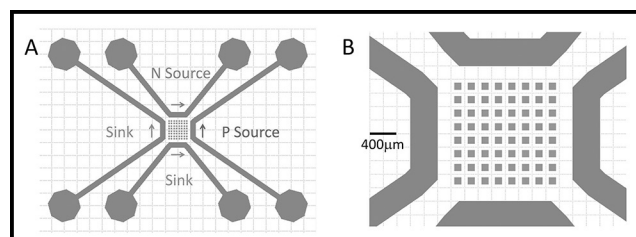


Figure 1: Dual-gradient microfluidic platform design. A. Top view of a device. B. A zoomed-in view of microhabitats and channel. The 8×8 array of $100 \mu\text{m}$ cubic habitats are separated by $100 \mu\text{m}$ from each other. These habitats are surrounded by four channels with width of $400 \mu\text{m}$ and height of $200 \mu\text{m}$. N source and P source runs through the top and right channel respectively, and the other channels are sink channels. A gradient is generated for each chemical species in the microhabitat array region through molecular diffusion.

In this project, we developed a microhabitat platform that can provide dual nutrient gradients to facilitate a more realistic condition found in nature. The design of our device is shown in Figure 1, which consists of 64 microhabitats in the form of an 8×8 array and each habitat is $100 \mu\text{m} \times 100 \mu\text{m} \times 100 \mu\text{m}$. The microhabitat array is surrounded by two sets of side channels each with the width of $400 \mu\text{m}$ and height of $200 \mu\text{m}$. In each set of side channels, we can run source media (with N, or P) and blank media respectively, and a stable gradient can be simultaneously generated along vertical and horizontal directions.

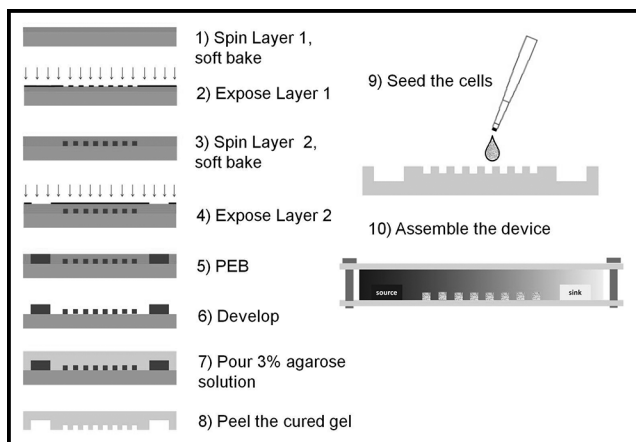


Figure 2: Schematics of a two-layer SU-8 photolithography procedure and the final microfluidic device assembly. First, a 100 μm resist layer was spun on a wafer, soft baked and exposed. Then, another 100 μm layer was spun on top and baked together overnight, followed by the second exposure and post exposure bake (PEB) for the 200 μm structures. The unexposed resist was then developed and the structures went through hard bake. For device assembly, the pattern was imprinted on an agarose gel, and cells were seeded in the microhabitats. The gel was then sandwiched between glass slide and manifolds and tightened by screws.

Soft lithography was used to make this dual-gradient microhabitat platform, which involves fabricating the silicon master mold and molding the pattern onto agarose gel for device assembly. Schematics of the step by step procedure are shown in Figure 2. The silicon master mold was fabricated using two-layer SU-8 negative resist photolithography, since the channels are 200 μm high and the microhabitats are 100 μm high. The post exposure bake (PEB) of the first layer of photo resist was combined with the soft bake of the second layer of the photo resist. Also, it was found that slow temperature ramping and relaxation time after each bake is critical to minimize internal stress in order to prevent resist detachment problem. After developing, the height of the feature was measured using the P10 profilometer, and a layer of FOTS was deposited using molecular vapor deposition (MVD 100) to increase the surface hydrophobicity for easier demolding of agarose gel. To transfer the pattern, boiled 3% agarose solution was poured on the silicon master and peeled once it cured. The gradient behavior of this dual-gradient platform was characterized using fluorescent dyes (for details see reference [3]).

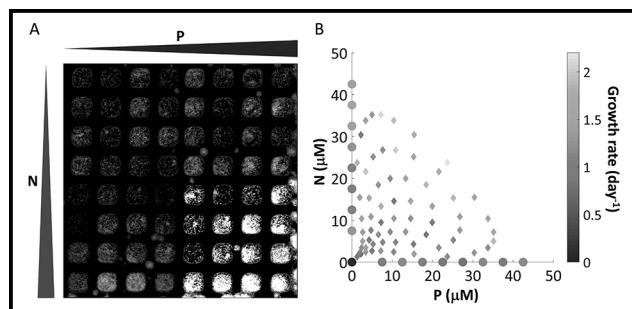


Figure 3: Growth of *C. reinhardtii* under nutrients (N, P) gradient. A. Fluorescence images of nutrients co-limited cells growing under N and P dual gradients at day 4. B. The growth rate of *C. reinhardtii* under: control condition, no N or P (dot at the origin), single P gradient (dots on x axis), single N gradient (dots on y axis), and dual-gradient (all the diamonds). Shade is coded for the value of the growth rate.

The platform was used to study the growth of *C. reinhardtii* under nitrogen (N) and phosphorous (P) gradients. Experiments with N, P co-limited cells showed that N and P synergistically promoted cell growth (Figure 3A), while no discernible response was observed when single N or P gradient was imposed [3]. Growth rates under single gradient, dual-gradients, and control conditions were obtained and organized in Figure 3B, which could benefit the quantitative study of microalgal growth. These results proved the enabling power of the dual-gradient microhabitat platform in screening effects of multiple environmental factors in photosynthetic cell growth [3].

References:

- [1] Paerl, Hans W., et al. Environmental Science and Technology (2018): 5519-5529.
- [2] Kim, Beum Jun, et al. Lab on a Chip 15.18 (2015): 3687-3694.
- [3] Liu, Fangchen, et al. Lab on a Chip 20.4 (2020): 798-805.

Metasurface-Enhanced Infrared Spectroscopy for Real-Time Measurement of Live Cells

CNF Project Number: 2472-16

Principal Investigator(s): Gennady Shvets

User(s): Steven He Huang, Po-Ting Shen, Jiaruo Li

Affiliation(s): Applied and Engineering Physics, Cornell University

Primary Source(s) of Research Funding: Cornell University internal funding

Contact: gs656@cornell.edu, hh623@cornell.edu, ps944@cornell.edu, jl2596@cornell.edu

Website: <http://shvets.aep.cornell.edu>

Primary CNF Tools Used: JEOL 9500, SC4500 evaporator, Zeiss Supra SEM, PDMS casting station, Anatech resist strip

Abstract:

Infrared (IR) spectroscopy for the label-free, nondestructive analysis of biological samples is a rapidly expanding area of research. When combined with multivariate statistical analysis and machine learning techniques, IR spectroscopy has been shown to be a powerful tool that can distinguish different types of tissues and cells. However, current applications of IR spectroscopy for live cells are limited due to the strong attenuation of IR light in water. In our lab, we have developed Metasurface-Enhanced Infrared Spectroscopy (MEIRS) as a novel tool to perform spectral analysis of live cells in standard cell culture conditions. The cells are cultured on plasmonic nanoantennas (metasurface), and the plasmonic hotspots are used to enhance the IR signal. We have used MEIRS to track the changes in the cells *in situ* as they are introduced to different stimuli. We are also investigating the combination of MEIRS with electrical-impedance sensing to create a multi-modal cellular assay.

Summary of Research:

Infrared (IR) spectroscopy is widely used to identify chemical compounds through their molecular vibration fingerprints.

Recently, IR spectroscopy has found applications in biological analysis as a tool for histology and cytopathology, identifying tumor tissues from normal tissues and monitoring the effect of chemotherapeutics on cancer cells. However, IR light is strongly attenuated in water, and thus traditional IR spectroscopy often involves fixing and drying the biological sample, limiting its utility as a cellular assay. We have developed a novel technique that we named metasurface-enhanced infrared spectroscopy (MEIRS) to measure live cells in physiological conditions.

In MEIRS, cells are seeded on a planar array of gold plasmonic nanoantennas called metasurfaces. These resonant nano-antennas support plasmonic hot spots in their vicinity, enhancing the light-matter interaction. The IR absorption signal from cells interacting with these plasmonic hot spots can be measured through the reflected light, overcoming the attenuation in water.

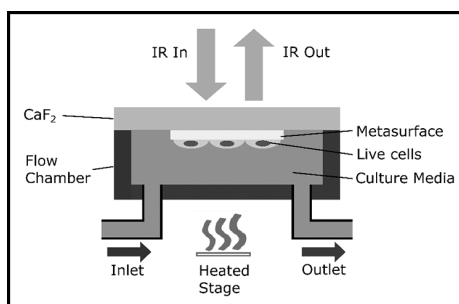


Figure 1: Schematic drawing of the flow-chamber setup for *in situ* IR spectroscopy of live cells.

In the past, we have used this metasurface for the IR spectroscopy of protein monolayers [1] as well as fixed and dried cells [2]. Our current work focus on further extending this technique to the measurement of live cells on the metasurface, monitoring their changes in response to different compounds.

The plasmonic metasurfaces are fabricated in the CNF cleanroom.

Metasurfaces are fabricated on IR-transparent CaF_2 substrates. First, patterns are defined on poly(methyl methacrylate) (PMMA) using electron beam lithography with the JEOL 9500 system. This is followed by gold evaporation and lift-off in acetone to create the gold nanoantennas.

Once the fabrication is done, Anatech resist strip is used to clean the metasurface and remove any resist residues. To perform *in situ* spectroscopy with live cells, we use a polydimethylsiloxane (PDMS) based flow chamber to maintain physiological conditions, which is also fabricated at the CNF. A schematic drawing of our measurement setup is shown in Figure 1.

Human squamous carcinoma cell line A431 cells were seeded on metasurfaces coated with fibronectin. Scanning electron microscope (SEM) images of the cells on the metasurface (Figure 2) shows that the cells preferentially attach to the gold nanostructures rather than the CaF_2 substrate. The interaction between the cells and the metasurface is still under investigation, but cellular attachment on gold nanoantennas implies that there is a significant spatial overlap between the plasmonic hotspot and the cells, which can lead to a strong enhancement in the detected signal.

We have monitored the response of A431 cells to 10 mM methyl-beta-cyclodextrin (MBCD), a compound known to extract cholesterol from the cellular membrane. The result was analyzed by principal component analysis (PCA) followed by promax rotation (Figure 3). Two different cellular processes, with different spectral features as well as temporal dynamics, can be seen. We attribute component 1 to the detachment of adhesion sites from the metasurface, while component 2 is thought to reflect changes in IR light scattered by the cells due to changes in cell morphology. We also found significant changes in the IR absorption from lipids right after MBCD was added to the flow chamber, which is attributed to the cholesterol extraction from the cellular membrane.

We are also investigating the combination of electrical impedance-based measurement with our metasurface-enhanced spectroscopy. The cell electrical impedance sensing (ECIS) is a proven technique to monitor *in situ* cell behaviors. The technique involves growing the cells on a surface with patterned microelectrodes and monitoring the changes in electrical impedance as the cells undergo certain changes.

Figure 4 shows A431 cells on the microelectrodes on our prototype device. The electrodes are connected to an impedance analyzer (we use an oscilloscope for preliminary tests) that uses AC voltage to measure the voltage and current across the attached cells. The electrodes of ECIS must be patterned in a specific way such that the attached cells block the current between electrodes. Different phases of cell attachment, spreading, migration, and proliferation can be distinguished through the change in impedance. We believe that although both ECIS and MEIRS detect phenotypical changes in the cells, there is a subtle difference in their signal, and this could provide more insight into the biological processes occurring in the cells.

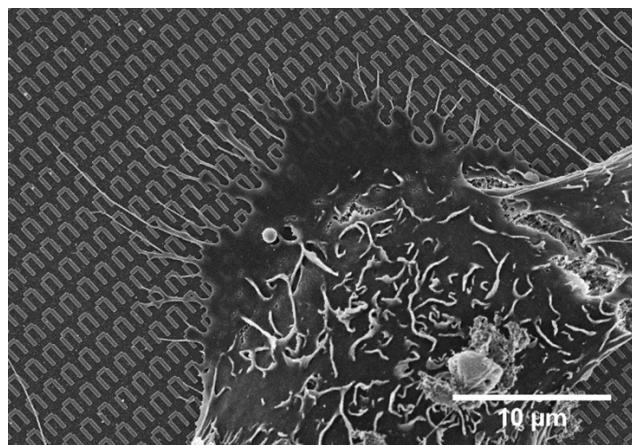


Figure 2: SEM image of A431 cells grown on the plasmonic metasurface.

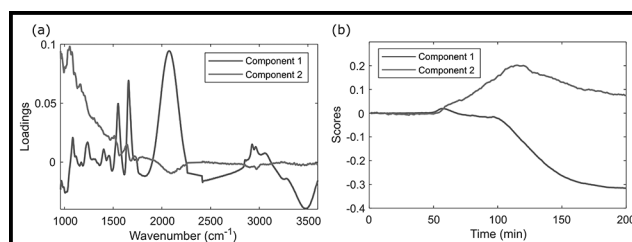


Figure 3: The spectral changes of A431 cell in response to MBCD. The results were analyzed using PCA, followed by promax rotation. (a) Component loadings and (b) the associated component scores. MBCD arrives at the flow chamber at approximately $t = 45$ min.

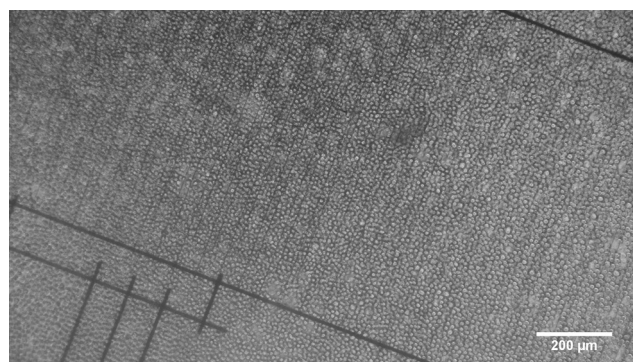


Figure 4: A431 cells on a microelectrode-patterned surface for electrical impedance measurement.

References:

- [1] Wu, C., et al. Fano-resonant asymmetric metamaterials for ultrasensitive spectroscopy and identification of molecular monolayers. *Nat. Mater.* 11, 69-75 (2011).
- [2] Kelp, G., et al. Application of metasurface-enhanced infra-red spectroscopy to distinguish between normal and cancerous cell types. *Analyst* 144, 1115-1127 (2019).

Retinal Implant Project

CNF Project Number: 2504-16

Principal Investigator(s): Douglas Shire, Ph.D.^{1,3,4}

User(s): Marcus Gingerich, Ph.D.^{1,4}, Patricia Wong^{2,4}

Affiliation(s): 1. Dept. of Electrical Engineering, Cornell University; 2. Dept. of Neuro-Ophthalmology, Massachusetts Eye and Ear Infirmary; 3. VA Cleveland Healthcare System; 4. Bionic Eye Technologies, Inc.

Primary Source(s) of Research Funding: NIH/NIBIB U01EB018873; NIH/NIBIB R01EB022013, NIH R43 NS113708-01 Massachusetts Lions Eye Research Fund, DoD W81XWH-16-2-0015

Contact: dbs6@cornell.edu, mdg37@cornell.edu, pwong@bionicvisiontechnologies.com

Website: <http://www.bostonretinalimplant.org>

Primary CNF Tools Used: PT-72, Lithography toolset/MA6, DWL2000, evaporators, AJA sputter, Gamma spray coater, SEMs, gold electro-plating, Class 2 lithography toolset, Oxford PECVD, Oxford 100 etcher, Oxford Cobra etcher, Glenn 1000, YES polyimide oven, Parylene-C coater, VersaLaser, numerous metrology tools

Abstract:

The purpose of the Retinal Implant Project is to restore useful vision to patients who are blind with degenerative retinal diseases. The primary illnesses we hope to treat are retinitis pigmentosa (a primary cause of inherited blindness) and age-related macular degeneration (the leading cause of blindness in the developed world). Both these diseases cause the eventual destruction of the photoreceptor cells — rods and cones — in the retina, leaving intact the ganglion cells, which transmit electrical impulses (and hence visual information) to the brain. The ganglion cells may be stimulated, however, with biphasic current pulses from a microfabricated electrode array. Blind surgical volunteers have consistently described visual percepts that resulted from such stimuli, and this has led our team to develop a wireless, implantable retinal prosthesis.

Summary of Research:

The implanted portion of our device consists of power and data secondary receiving coils, and — in a sealed Ti can — a small number of discrete components, and a custom designed application specific integrated circuit (ASIC), which consists of circuitry for clock and data recovery, current drivers for electrodes in a stimulating electrode array, and a programmable function generator capable of stimulating with a wide range of pulse widths and amplitudes. The current outputs drive high-charge capacity sputtered iridium oxide film (SIROF) stimulating electrodes, which in turn give rise to the visual percepts mentioned above.

CNF-fabricated components of this system have included various proof-of-concept test structures and tools used in the research effort and an integrated combination flexible circuit and stimulating electrode array. Si wafers serve as carriers for these freestanding films during processing. The electrode leads are fabricated inside of 'sandwiches' of polyimide and amorphous silicon carbide (SiC), while the SIROF electrodes are reactively sputter-deposited.

Assembly of the intraocular components of the prosthesis is accomplished by flip chip solder ball bonding of the IC and solder attachment of discrete components onto an internal flexible circuit board which is hermetically sealed into an ultraminiature Ti can. The RF coils are soldered and glued to the integrated external flex-array which is in turn thermosonically bonded to the hermetic feedthrough of the Ti can. Finally, the thermosonic bonds are protected and insulated with an over-mold. An external patient interface unit, will consist of a video camera for capturing images, a digital signal processor, and a radio frequency (RF) transmitter and coil to relay power and data to the implanted device.

Scientific challenges still remain in realizing a chronically implantable retinal prosthesis. While our first-generation device was primarily encapsulated in polymers for short term proof-of-concept implant studies, our second-generation system focused on a system which would last many years *in vivo*. Our more recent efforts have focused on developing a device with 256+ stimulation channels which is still small enough

and of a configuration to be easily implanted in the ocular orbit and continue to function for many years *in vivo*. Thus, a major effort has been the development of a technological platform to build a robust, hermetically packaged, high-density subretinal visual prosthesis with a lifetime of > ten years in biological saline that is scalable to hundreds of I/O channels.

Recent efforts have focused on improvements in assembly techniques, under-filling, overmolding and final Parylene-C protection, using the Parylene coater, have yielded a passive retinal implant system which has been successfully implanted in an animal model for several months with no significant adverse effects. Figures 1 and 2 show an example of the implant mounted on a model eyeball.

Other efforts at the CNF have included developing a microfabrication process for penetrating electrodes for long-term implantation in brain tissue. The goal is to extend the existing retinal stimulator platform to include electrodes which can be placed at different points in the visual tract to enable the restoration of sight due to other causes of blindness. These electrodes can be placed into structures such as the lateral geniculate nucleus (LGN) to produce visual signals at that location. The LGN is a structure located deeper within the brain thus a system of implanting the electrode array into the target location has had to be developed as well. A prototype insertion device, shown in Figure 3, includes a protective split-sheath inserter, the actual electrode array/signal cable and the insertion rod. The resulting system has the potential to be utilized in other applications such as those requiring deep brain stimulation including Parkinson's disease, severe depression, morbid obesity, and obsessive-compulsive disorder, to name a few.

References:

- [1] J. F. Rizzo, J. Wyatt, J. Loewenstein, S. Kelly, and D. Shire, "Methods and Perceptual Thresholds for Short-Term Electrical Stimulation of Human Retina with Microelectrode Arrays," *Investigative Ophthalmology and Visual Science*, vol. 44, no. 12, Dec. 2003, pp. 5355-5361.

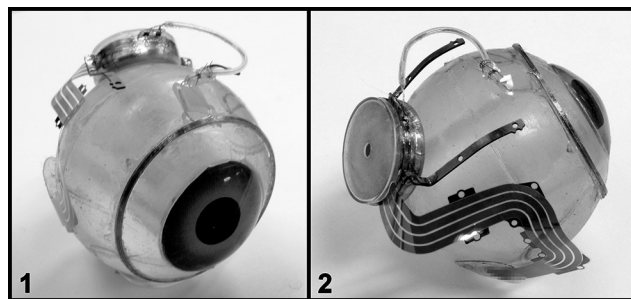


Figure 1, left: A side-frontal view of a passive retinal implant assembly is shown on an eyeball demonstrating the location of the power and data coil around the front of the eye. Figure 2, right: A side-rear view of a retinal implant assembly mounted is shown on an eyeball demonstrating the location of the hermetic titanium case and the stimulating electrode array at the back of the eye. (See pages vi-vii for full color versions of both images.)

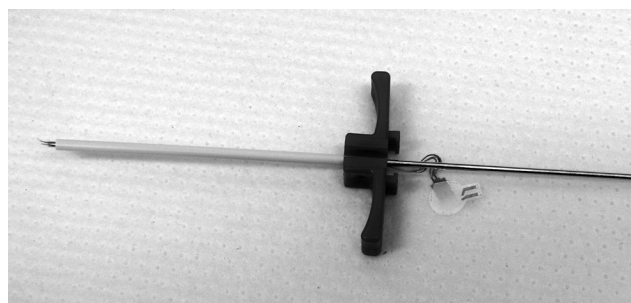


Figure 3: A prototype deep brain insertion sub-assembly is shown which includes a protective split-sheath inserter, the actual electrode array/signal cable and the tungsten insertion rod.

Circulating Extracellular Vesicles and Physical Stress in ME/CFS

CNF Project Number: 2590-17

Principal Investigator(s): Maureen R. Hanson, Ludovic Giloteaux

User(s): Ludovic Giloteaux

Affiliation(s): Department of Molecular Biology and Genetics, Cornell University, Ithaca NY

Primary Source(s) of Research Funding: NIH U54

Contact: mrh5@cornell.edu, lg349@cornell.edu

Website: <https://neuroimmune.cornell.edu/research/vesicles-and-signaling/>

Primary CNF Tools Used: Malvern NS300 NanoSight

Abstract:

Myalgic Encephalomyelitis/Chronic Fatigue Syndrome (ME/CFS) is a disabling illness affecting approximately two million Americans, with symptoms including extreme fatigue, pain, unrefreshing sleep, orthostatic intolerance, and cognitive difficulties. There is evidence for abnormal immune cell function and cytokine signaling. Some of the abnormalities in immune response may be due to altered cell-to-cell communication by extracellular vesicles released by immune cells and other cell types in the body. We are measuring number and size of vesicles per volume of plasma in order to detect any differences between ME/CFS patients and controls. Furthermore, we are using this information in order to normalize measures of protein and miRNA cargo between individual samples.

Summary of Research:

The Nanoparticle Tracking Analysis (NTA) instrument Malvern NS300 NanoSight was used for the sizing and quantification of extracellular vesicles (EVs) isolated from plasma samples from subject with ME/CFS and healthy individuals. Samples were obtained from individuals recruited at Ithaca College, New York City, and California within an NIH U54 project. Other samples were directly sent to us from Jackson Laboratory as a collaborative project funded by the NIH. We have measured size and numbers to inform Jackson Laboratory for experiments in which the EVs are mixed with cultured cells to observe effects on their function.

We studied an initial set of 70 samples, shown in Fig.1.

A manuscript is currently in preparation that will describe data concerning size, concentration, and cargo in EVs from these samples. There was no difference in the average size or total concentration of EVs between samples from ME/CFS patients vs. controls. A significant increase in the concentration of the 30-130 nm class of EV (exosome type) was observed in the ME/CFS samples in comparison to healthy controls (Figure 1C).

Conclusions and Future Steps:

We are periodically receiving additional samples from Ithaca College, Weill Cornell Medicine, and Los

Angeles, where subjects are performing two successive cardiopulmonary exercise tests. We are measuring size and numbers of EVs in plasma before and after such tests, and analysis of cargo in the EVs is underway.

The rationale behind this study is that it is known that EVs increase in blood following exercise by healthy people, and ME/CFS patients are known to have an abnormal response to exercise.

References:

- [1] Giloteaux L., A. O'Neal, S.M. Levine, J. Jesus Castro-Marrero, and M.R. Hanson. Cytokine profiling of plasma extracellular vesicles in individuals with Myalgic /Chronic Fatigue Syndrome. Oral presentation by L. Giloteaux at the meeting "Accelerating Research on ME/CFS," held at the NIH, Bethesda, MD on April 4-5, 2019.
- [2] Giloteaux, L., J. Castro-Marrero, A. O'Neal, J. Grenier, S. Levine, and M.R. Hanson. Cytokine and miRNA profiling of plasma extracellular vesicles in individuals with Myalgic Encephalomyelitis/Chronic Fatigue Syndrome. Poster presentation by L. Giloteaux at the International Society of Extracellular Vesicles (ISEV) 2019 conference held in Kyoto, Japan, April 23rd-28th.

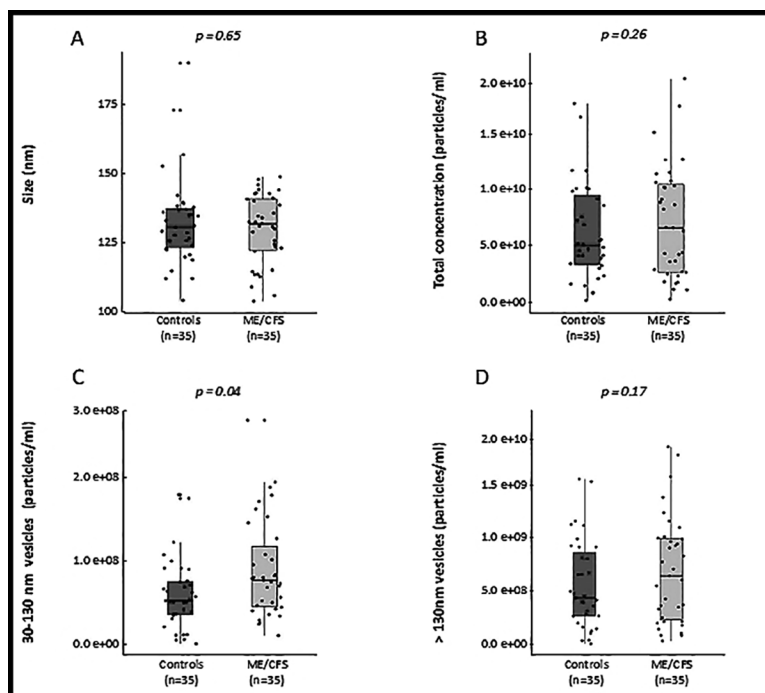


Figure 1: Characterization of EVs by Nanoparticle Tracking Analysis. Size in nanometers (A), total concentration of particles per ml of plasma (B), and the range of concentrations of 30-130 nm vesicles (C) and > 130 nm vesicles (D).

***In Vitro* Three-Dimensional Engineered Cardiac Tissue Mechanical Stimulation Platform**

CNF Project Number: 2619-17

Principal Investigator(s): Jonathan Butcher

User(s): Gaetano Scuderi

Affiliation(s): Biomedical Engineering Department, Cornell University

Primary Source(s) of Research Funding: National Institutes of Health

Contact: jtb47@cornell.edu, gjs95@cornell.edu

Website: <http://www.butcherlab.com/>

Primary CNF Tools Used: Objet30 Pro 3D printer, Parylene coater, VersaLaser engraver/cutter tool

Abstract:

People who suffer from heart failure have low survival rates since no clinically available cardiac regeneration therapy exists. However, one promising approach is the implantation of tissue engineered myocardium, but due to their immaturity they do not lead to any significant heart function improvements. To improve the maturity of the engineered cardiac tissues (ECT), researchers have attempted to mimic *in vivo* mechanical stimuli. However, current systems have major limitations that lead to only modest improvements in ECT maturity. Therefore, our objective was to develop a superior *in vitro* cardiac tissue platform and mechanical stimulation bioreactor system to ultimately study how various mechanical stimuli affect ECT maturity. Here, we demonstrate the successful development of a novel *in vitro* platform and bioreactor system. We hope to apply this novel system to develop more mature ECTs that can be translated clinically as a viable cardiac regeneration option.

Summary of Research:

In the United States, 750,000 Americans suffer from heart attacks annually with 16% of all cases leading to mortality [1]. Due to the inability for adult mammalian hearts to regenerate, the infarcted region becomes a fibrotic, non-contractile tissue which often leads to congestive heart failure [2]. The gold standard treatment option is heart transplantation, which has major limitations such as an inadequate supply, high risk of donor heart rejection/failure, and need for lifelong immunosuppressants.

Currently, no viable clinical cardiac regenerative therapy is available to restore heart function following a heart attack [3]. One promising cardiac regeneration approach involves the implantation of tissue engineered myocardium to restore heart function. Current tissue engineered myocardium, however, has been unsuccessful at restoring heart function due to the tissue's immature phenotype that has low survivability and poor host integration in adult hearts [3].

Therefore, researchers have turned to investigating ways to improve tissue engineered myocardium maturity that will better integrate with the host tissue. Mechanical stimulation utilizing mechanical anchorage to induce passive tension, passive stretch, and dynamic cyclic stretch have all shown to lead to modest improvements in

engineered cardiac tissue (ECT) maturity [4]. However, the current bioreactor systems have many limitations. All systems that dynamically stretch their ECT to mimic *in vivo* mechanical stimuli utilize stiff anchorage points, which prevents the tissues from producing work and can lead to an upregulation of pathological fibrosis/hypertrophic signaling [5]. Likewise, these bioreactor systems often use non-physiological stretching regimens that do not accurately recapitulate normal cardiac development, where a progressive increase in cardiogenic stretch patterns occur to lead to intrinsic maturity improvements [3].

For this project, our objective was to develop a high-throughput *in vitro* ECT platform system and mechanical stimulation bioreactor that allows for the following: 1) anchorage points that allow for contraction and work production, 2) mechanically stretch over a wide range of strain magnitudes (0-50%) and rates (1-5 Hertz), and 3) high-throughput stimulation of 48 ECTs with varying strain magnitudes simultaneously.

Our *in vitro* ECT platform required precise manufacturing of an intricate geometric mold and therefore we turned to Cornell NanoScale Facility's Objet30 Pro 3D printer. This design provided the ability to cast polydimethylsiloxane (PDMS) post constructs that serve as nearly perfectly

elastic bioinert anchorage points. PDMS serves as a reliable candidate for ECTs due to its elastic properties, which allows the tissues to contract/deflect the material and therefore produce work [3]. Our ECTs can be cultured on these PDMS constructs (Figure 1).

This PDMS post design allows us to control the bending stiffness that the tissue experiences by restricting any z-direction movements during contractions and serves as a means for the tissue to be stimulated by deflecting the post from above the tissue using a customized mechanical stimulation bioreactor. We validated our platform’s ability to create functional ECTs by culturing primary fetal chick cardiac cells on our post platform and compared them to unloaded (non-anchored) control tissues. The loaded ECTs demonstrated aligned cardiomyocytes and non-cardiomyocytes along the axis of tension while the unloaded controls had no inherent alignment (Figure 2).

Our custom high-throughput uniaxial mechanical stimulation bioreactor system for stimulating 48 tissue constructs on a standard 48 well plate was developed using the Objet30 Pro 3D printer (Figure 3). The system uses a hybrid external stepper motor linear actuator. As the linear actuator translates, it moves a customized 3D printed part attached to a steel rod that is attached inside the customized 3D printed box that sits on top of the 48-well plate. A tab grid system then slides along the 3D printed box’s linear track and deflects the PDMS posts just above the tissues to apply a stretch. The amount of stretch can easily be modulated using an Arduino Uno system. Likewise, different tab grid systems have been developed that are offset by certain lengths and thus can apply various strains ranging from 0-50% across the 48-well plate simultaneously.

Our next steps are to test out our design by culturing various ECTs and stretching our tissues with varying stretch regimens to determine what types of regimens provide the greatest improvements in cardiac tissue maturity.

References:

- [1] Mozaffarian, D., et al. Heart disease and stroke statistics—2016 update a report from the American Heart Association. *Circulation* 133, e38-e48 (2016).
- [2] Alcon, A., Cagavi Bozkulak, E., and Qyang, Y. Regenerating functional heart tissue for myocardial repair. *Cellular and Molecular Life Sciences* 69, 2635-2656 (2012).
- [3] Scuderi, G., and Butcher, J. Naturally engineered maturation of cardiomyocytes. *Frontiers in Cell and Develop. Bio.* 5, (2017).
- [4] Radisic, M., et al. Biomimetic approach to cardiac tissue engineering. *Philos. Trans. R. Soc. B Biol. Sci.* 362, 1357-1368 (2007).
- [5] Leonard, A., et al. Afterload promotes maturation of human induced pluripotent stem cell derived cardiomyocytes in engineered heart tissues. *J. Mol. Cell. Cardiol.* 118, 147-158 (2018).

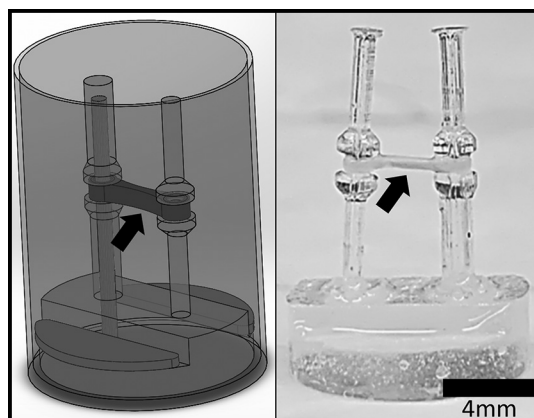


Figure 1: SolidWorks schematic of PDMS construct (left) and fixed ECT after one-week culture on PDMS construct (right). Black arrows point to ECTs.

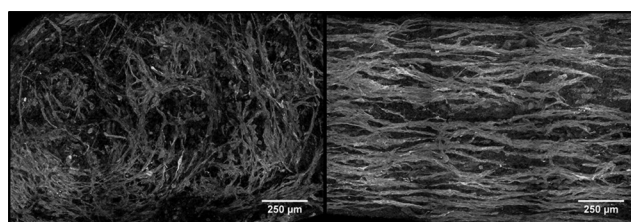


Figure 2: Whole mount immunohistochemical staining of unloaded (left) and loaded (right) ECTs stained for non-cardiomyocytes (red), cardiomyocytes (green), and nuclei (blue). (See pages vi-vii for full color version.)

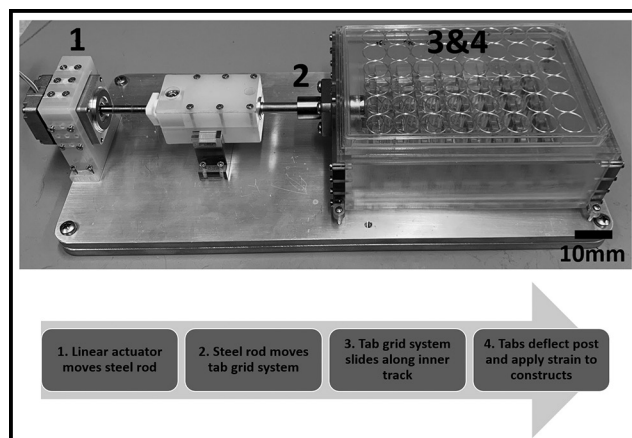


Figure 3: Bioreactor (top) and flow chart of bioreactor operation (bottom).

Evaluating the Role of Tumor-Derived Extracellular Vesicles in Breast Cancer

CNF Project Number: 2706-18

Principal Investigator(s): Lara Estroff

User(s): Minjee Kang

Affiliation(s): Materials Science and Engineering, Cornell University

Primary Source(s) of Research Funding: Human Frontier Science Program

Contact: lae37@cornell.edu, mk2546@cornell.edu

Primary CNF Tools Used: Malvern NS300 NanoSight

Abstract:

Breast cancer frequently metastasizes to bone where it leads to osteolytic bone degradation and poor clinical prognosis. Nevertheless, therapeutic options to interfere with this process are scarce as the underlying mechanisms remain unclear. Previous studies showed that primary breast cancer tumors can alter bone materials properties and bone metastasis even prior to secondary tumor formation, suggesting possible interference with bone mineralization pathways [1]. It is well-known that extracellular vesicles (EVs) shed from tumor cells enter circulation and act as satellites of information transfer among cells. It is unknown, however, if circulating breast tumor-shed EVs contribute to early-stage changes of bone microenvironment. Our project investigates the connections between EV generation, breast cancer malignancy, the binding affinity of EVs in metastatic sites such as the bone.

Summary of Research:

We investigated how tumor-shed EVs interact with a bone-mimetic microenvironment, specifically mineralized collagen fibrils with poorly crystalline apatite crystals, and if EVs bound to the bone-like matrix can promote tumor cell binding to the bone extracellular matrix (ECM). To study interaction between tumor-shed EVs and bone ECM *in vitro*, we prepared bone-mimetic scaffolds composed of mineralized collagen type I fibrils fabricated using a polymer-induced liquid-precursor process.

We used the CNF NanoSight instrument to analyze the size distributions and measure concentrations of EVs shed by breast cancer cell lines. Our findings in Figure 1 indicate that compared to their benign counterparts, cell lines that represent more invasive and metastatic potential shed a greater amount of EVs per cell, with increases in both microvesicles and exosomes.

Next, we loaded labelled tumor-shed EVs into the scaffolds and examined the degree of binding of EVs to the collagen fibrils using confocal microscopy and SEM. The distribution and degree of binding of EVs in the matrix were correlated with various factors including breast tumor cell malignancy, the presence of mineral, and size of EVs. Breast-tumor shed EVs successfully adhered to the bone matrix via ligand-receptor interactions where the degree of binding was dependent upon tumor cell malignancy and vesicle size.

EVs adhered slightly better on non-mineralized scaffolds than mineralized scaffolds but the difference was nonsignificant. EVs shed from more malignant breast tumor cells were more effective in binding by 3-8 times to the matrix than those from less malignant cells as shown in Figure 2.

Conclusions and Future Steps:

The adhesion of breast tumor-shed EVs to the bone ECM is associated with their size and parent cell malignancy *in vitro*. These findings suggest a potential role for tumor-shed EVs in preparing a pre-metastatic niche within the bone ECM to which tumor cells are attracted. We anticipate that new understanding of adhesion ability of tumor-shed EVs to the bone ECM will contribute to our understanding of role of EVs in breast cancer bone metastasis.

References:

- [1] He F, Chiou AE, Loh HC, Lynch ME, Seo BR, Song YH, Lee MJ, Hoerth R, Bortel E, Willie B, Duda G, Estroff LA, Masic A, Wagermaier W, Fratzl P, Fischbach C. Multiscale characterization of the mineral phase at skeletal sites of breast cancer metastasis. *Proc. of the National Academy of Sciences*, 114(40), 10542-10547. <https://doi.org/10.1073/pnas.1708161114> (2017).

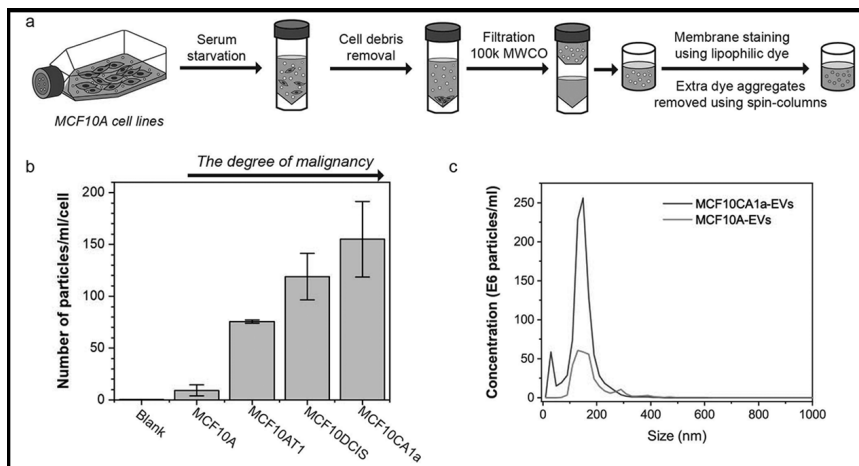


Figure 1: (a) Schematic representation of the collection of extracellular vesicles (EVs). Subconfluent MCF10A cell lines were cultured and serum-starved for 24 h. Media were collected, centrifuged to remove cell debris, and then filtered to concentrate EVs. Fluorescent lipophilic dyes were used to stain membranes of EVs, and the extra aggregates of dyes were removed using spin-columns. (b) Concentration of particles collected from the series of MCF10A cell lines as measured by NanoSight. (c) Size distribution of particles shed from MCF10A cells and MCF10CA1a cells as measured by NanoSight.

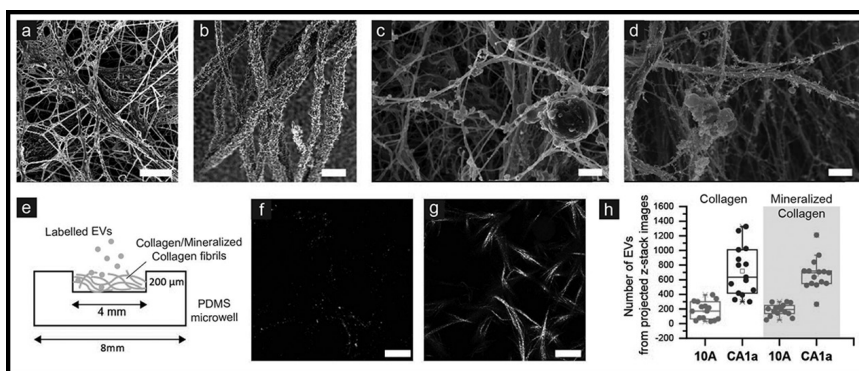


Figure 2: Binding of EVs onto 3D bone-mimetic scaffolds. (a-d) Representative SEM images showing the microstructure of (a) collagen, (b) mineralized collagen prepared via a polymer-induced liquid-precursor process, and MCF10CA1a-shed EVs bound onto (c) collagen fibrils, and (d) mineralized collagen fibrils. Scale bars = 10 μm. (e) Schematic of the bone-mimetic scaffolds used in this study. Collagen or mineralized collagen fibrils were cast into poly(dimethylsiloxane) (PDMS) microwells and fluorescently labeled EVs were incubated into the wells. (f, g) Confocal microscopy images of (f) labeled EVs in green channel and (g) collagen network in reflection mode. (h) Quantification of confocal images to compare the levels of EVs shed from MCF10A cell lines and MCF10CA1a cell lines bound onto collagen and mineralized collagen.

Fabrication of Biological Superhydrophobic Surfaces

CNF Project Number: 2727-18

Principal Investigator(s): Sunghwan Jung

User(s): Ehsan Esmaili

Affiliation(s): Biological and Environmental Engineering, Cornell University

Primary Source(s) of Research Funding: Startup funding

Contact: sj737@cornell.edu, ee287@cornell.edu

Primary CNF Tools Used: ABM aligner, photolithography room

Abstract and Summary of Research:

The CNF photolithography technique has been used to fabricate a microstructure to study the rainfall on biological superhydrophobic surfaces. In this work, we explored raindrop impact at high speeds, which exhibits unexpected drop dynamics: numerous shock-like waves are generated on a spreading drop in the presence of microscopic textures on biological surfaces. Then, the spreading drop with shock-like waves is fragmented soon after it approaches a maximal spreading extent, thereby reducing the residence/contact time more than twofold.

One paper has been prepared and submitted to the PNAS journal, titled as "Shock-like waves and drop fragmentation of a raindrop impacting biological surfaces."

Development of Heparin-Based Coacervate Loaded Liposomes as a Non-Invasive Therapy for Myocardial Infarction

CNF Project Number: 2754-18

Principal Investigator(s): Yadong Wang

User(s): Chia-Wei Yeh

Affiliation(s): Biomedical Engineering, Cornell University

Primary Source(s) of Research Funding: Cornell Startup Funds

Contact: yw839@cornell.edu, cy465@cornell.edu

Primary CNF Tools Used: ABM contact aligner

Abstract:

Cardiovascular disease is one of the major leading causes of death worldwide. Specifically, myocardial infarction (MI), generally known as heart attack, is the main cause of death in cardiovascular disease. Among them, the major cause of death of MI is due to the myocyte necrosis and heart failure. Therefore, it is of particular importance to prevent myocyte necrosis after MI as well as induce infarcted heart tissue to regenerate.

Coacervate is an electrostatically bound complex between cationic and anionic polyelectrolytes. In the extracellular matrix (ECM), glycosaminoglycan such as heparan sulfate proteoglycan (HSPG) binds with several growth factors (GFs) to form HSPG-GF complex. This complex not only serves as reservoir for bonding and stabilization of GFs but also potentiates GFs responsible for maintaining normal cellular function. Due to the similar mechanism of protein-extracellular matrix interaction, it has been shown that heparin-based coacervate is a promising candidate for drug delivery system in biomedical and tissue engineering applications. However, coacervate complex is unstable in the blood stream owing to the relatively weak electrostatic interaction within coacervate droplets, leading to the difficulty to systemically administer coacervate via intravenous injection.

To solve this problem, we aim to encapsulate heparin-based coacervate complex into liposome, namely coacervate vesicles or covesicles in short, for a non-invasive therapy for MI. In this study, polyanion heparin is utilized to complex with vascular endothelial growth factors C (VEGF-C) to form heparin-growth factor complex, which is then mixed with synthetic polycation, poly(ethylene arginyl aspartate diglyceride) (PEAD) to construct VEGF-C loaded coacervate droplets. In order to enhance coacervate complex stability in the blood stream, an on-chip microfluidic device is used to generate covesicles by encapsulating VEGF-C loaded coacervates into liposomes in a well-defined manner. The therapeutic effect of the covesicles will be evaluated on rat myocardial infarction model.

Summary of Research:

Covesicles are successfully generated in the designed microfluidic chip utilizing three phases: outer aqueous phase (OA), inner aqueous phase (IA), and lipid carried organic phase (LO), as shown in Figure 1 and Figure 2. OA contains 15% (vol/vol) glycerol and 5% (w/v) P188 in water, IA contains 15% (vol/vol) glycerol and PEAD/heparin coacervate complex in water, and LO contains 0.2% (wt/vol) DOPC in 1-octanol. Coacervate complex is formed by mixing PEAD solution and heparin solution prior to flow into microfluidic chip.

From Figure 1 and 2, PEAD/heparin coacervate complex is encapsulated by 1-octanol, forming water-in-oil droplets, then further pinched off by OA solution, and forming water-in-oil-in-water double emulsion droplets at the post-junction area. Moreover, covesicles with uniform size and high encapsulation efficiency are observed under the following flow rate: OA: 900 $\mu\text{L/hr}$, IA: 30 $\mu\text{L/hr}$, LO: 30 $\mu\text{L/hr}$, as shown in Figure 3. The average diameter of covesicles is 17.87 μm .

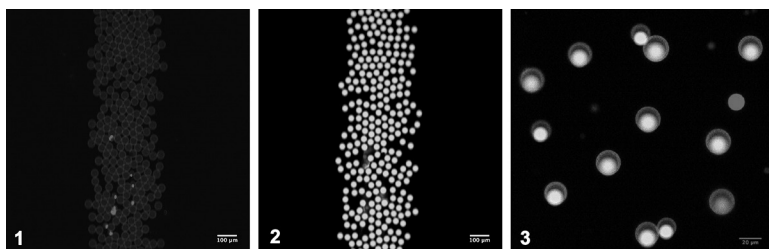


Figure 1, left: Rhodamine-labeled liposome formed via the designed microfluidic device. Flow rate: OA: 300 $\mu\text{L/hr}$, IA: 30 $\mu\text{L/hr}$, LO: 30 $\mu\text{L/hr}$. Scale bar: 100 μm .
Figure 2, middle: FITC-labeled PEAD/heparin coesicles encapsulated in liposome via the designed microfluidic device. Flow rate: OA: 300 $\mu\text{L/hr}$, IA: 30 $\mu\text{L/hr}$, LO: 30 $\mu\text{L/hr}$. Scale bar: 100 μm .
Figure 3, right: Coesicles with uniform size and high encapsulation efficiency. Red: rhodamine-labeled lipid. Green: FITC-labeled heparin. Flow rate: OA: 900 $\mu\text{L/hr}$, IA: 30 $\mu\text{L/hr}$, LO: 30 $\mu\text{L/hr}$. Scale bar: 100 μm . (See pages vi-vii for full color versions of all three images.)

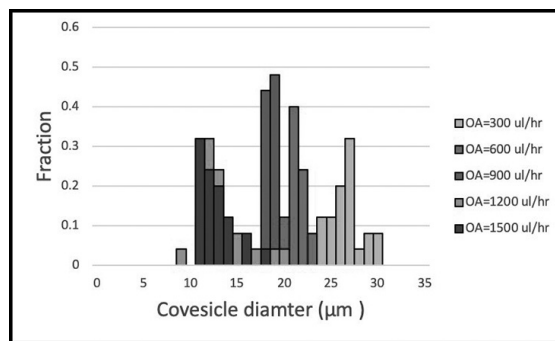


Figure 4: Coesicles diameter distribution vs. OA flow rate.

We are also interested in generating coesicles with various size. Thus, via using different flow rate, the diameter of coesicles ranges from 30 μm to 10 μm is achieved, as shown in Figure 4.

In order to achieve dripping regime during coesicles generation, both of IA and LO flow rate is maintained at 30 $\mu\text{L/hr}$. As expected, the diameter of coesicles decreases when OA flow rate increases. In our proposed strategy, coesicles less than 10 μm in diameter is our major target.

For next step, we will move forward to encapsulate VEGF-C into coesicles and test the protection effect on VEGF-C.

References:

- [1] Deshpande, S., and C. Dekker. "On-chip microfluidic production of cell-sized liposomes." *Nature protocols* 13.5 (2018): 856.
- [2] Deshpande, S., et al. "Spatiotemporal control of coeservate formation within liposomes." *Nature Com.* 10.1 (2019): 1800.

Characterization of E0771 Exosomes

CNF Project Number: 2780-19

Principal Investigator(s): Cynthia Leifer

User(s): Jingyi Chen, Christopher Wan

Affiliation(s): Microbiology and Immunology, Cornell University

Primary Source(s) of Research Funding: PSOC Pilot Project Funding

Contact: cynthia.leifer@cornell.edu, jc2876@cornell.edu, cw685@cornell.edu

Primary CNF Tools Used: NanoSight

Abstract:

Pathologic activation of the blood clotting system in cancer is associated with systemic thrombotic events as well as transformation, growth and metastasis of various tumors [1,2]. Coagulation is activated primarily by tissue factor (TF). TF is overexpressed in breast tumors *in situ* and in breast cancer cell lines, particularly triple negative cells [3,4]. Overexpression of TF in patient tumors correlates with a poor prognosis [3]. Cancer cells and the tumor microenvironment induce a protumorigenic, pro-angiogenic, and immunosuppressive phenotype in tumor-associated immune cells like macrophages [9]. It is unknown whether breast cancer cell-generated TF-coagulation complexes and PARs regulate macrophage recruitment to tumors or whether they subsequently modulate macrophage behavior in tumors. This is important since macrophage recruitment and regulation contributes to angiogenesis, metastasis and tumor progression [10-12].

We hypothesized that breast cancer-associated hemostatic components regulate macrophage recruitment and their inflammatory, angiogenic and hemostatic activity. To investigate this question, we determined that cancer-derived extracellular vesicles had intrinsic procoagulant activity and conferred that procoagulant activity to macrophages. A key part of our work was quality control of these extracellular vesicles that we subsequently used in our macrophage experiments. We used the NanoSight particle analyzer to characterize the extracellular vesicle populations purified from cancer cell-conditioned and control media. Data obtained using the NanoSight confirmed that we isolated particles 100-200 nm, compatible with extracellular vesicles. Altogether, our data show that breast cancer-derived microparticles confer procoagulant activity to macrophages, which may play a key role in the connection between coagulation and inflammation to regulate tumor growth and anti-tumor immunity.

Summary of Research:

In this project, we used the CNF NanoSight to perform quality control on our cancer-derived and control extracellular vesicles that were then used in additional experiments. Because of the NanoSight data, we demonstrated the procoagulant activity of a mouse breast cancer cell line and found that the vesicles derived from the cells accelerated clotting in mouse plasma.

Overnight incubation of a mouse macrophage cell line with the isolated vesicle fraction from tumor-conditioned, but not cell-free, media increased the procoagulant activity of the mouse macrophage cell line.

This supported our hypothesis that tumor cells upregulate procoagulant activity in macrophages. Our goal with using the Cornell NanoScale Facility was to characterize the size distribution of the obtained vesicles.

We found that the microvesicle fraction consisted of a dominant population of particles 100-200 nm, supporting successful isolation of various subsets of extracellular vesicles shed from tumor cells (Figure 1). These data supported several grant applications currently under review.

References:

- [1] Khan UT, Walker AJ, Baig S, et al. Venous thromboembolism and mortality in breast cancer: cohort study with systematic review and meta-analysis. *BMC Cancer* 2017; 17:747.
- [2] Cole M, Bromberg M. Tissue factor as a novel target for treatment of breast cancer. *Oncologist* 2013; 18:14-18.
- [3] Vrana JA, Stang MT, Grande JP, et al. Expression of tissue factor in tumor stroma correlates with progression to invasive human breast cancer: paracrine regulation by carcinoma cell-derived members of the transforming growth factor beta family. *Cancer Res* 1996; 56:5063-70.
- [4] Che SPY, Park JY, Stokol T. Tissue Factor-Expressing Tumor-Derived Extracellular Vesicles Activate Quiescent Endothelial Cells via Protease-Activated Receptor-1. *Front Oncol* 2017; 7:261.
- [5] Versteeg HH, Schaffner F, Kerver M, et al. Inhibition of tissue factor signaling suppresses tumor growth. *Blood* 2008; 111:190-9.
- [6] Bourcy M, Suarez-Carmona M, Lambert J, et al. Tissue Factor Induced by Epithelial-Mesenchymal Transition Triggers a Procoagulant State That Drives Metastasis of Circulating Tumor Cells. *Cancer Res* 2016; 76:4270-4282.
- [7] Palumbo JS, Talmage KE, Massari JV, et al. Tumor cell-associated tissue factor and circulating hemostatic factors cooperate to increase metastatic potential through natural killer cell-dependent and -independent mechanisms. *Blood* 2007; 110:133-141.
- [8] Eftekhari R, de Lima SG, Liu Y, et al. Microenvironment proteinases, proteinase-activated receptor regulation, cancer and inflammation. *Biol Chem* 2018; 399:1023-1039.
- [9] Aras S, Zaidi MR. TAMEless traitors: macrophages in cancer progression and metastasis. *Br J Cancer* 2017; 117:1583-1591.
- [10] Gil-Bernabé AM, Ferjancic S, Tlalka M, et al. Recruitment of monocytes/macrophages by tissue factor-mediated coagulation is essential for metastatic cell survival and premetastatic niche establishment in mice. *Blood* 2012; 119:3164-3175.
- [11] Lin L, Chen Y-S, Yao Y-D, et al. CCL18 from tumor-associated macrophages promotes angiogenesis in breast cancer. *Oncotarget* 2015; 6:34758-34773.
- [12] Su S, Liu Q, Chen J, et al. A positive feedback loop between mesenchymal-like cancer cells and macrophages is essential to breast cancer metastasis. *Cancer Cell* 2014; 25:605-620.

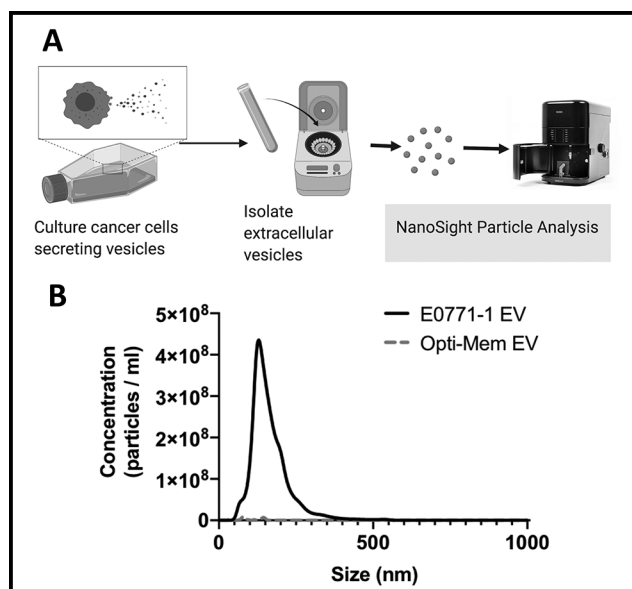


Figure 1: A) Schematic for nanoparticle isolation and analysis using the CNF NanoSight. Mouse mammary cancer cells (E0771) were cultured to produce extracellular vesicles (EV) in Opti-Mem media. Vesicles were isolated by differential centrifugation and subjected to NanoSight particle tracking analysis. B) Example NanoSight results of E0771 EV compared to media only EV preparations. These data demonstrate isolation of appropriate size EVs from cell cultures and not from media controls. These preparations were used in follow on experiments.

Microcontact Patterning of Single Cardiomyocytes on Shape Memory Polymers

CNF Project Number: 2806-19

Principal Investigator(s): Zhen Ma

User(s): Chenyan Wang

Affiliation(s): Bioengineering, Syracuse University

Primary Source(s) of Research Funding: Carol and Samuel Nappi Research Scholarship

Contact: zma112@syr.edu, cwang40@syr.edu

Website: <https://myheart.syr.edu/>

Primary CNF Tools Used: ABM contact aligner, Heidelberg mask writer-DWL2000

Abstract:

Investigating the mechanisms of cardiomyocytes remodeling in response to the dynamic mechanical environment is critical for understanding heart disease progression. The aim of our project is to develop a dynamic platform using shape memory polymers (SMPs) and pattern single cardiomyocytes on SMPs to observe their structural and functional remodeling induced by dynamic mechanical stress. To constrain single cardiomyocytes in a predefined shape, extracellular matrix (ECM) proteins need to be deposited on SMPs at the scale of single cell. Making use of the tools at Cornell NanoScale Science and Technology Facility (CNF), we successfully generated rectangular and square patterns at single-cell resolution on SU-8 coated silicon wafers. Using these wafer molds, we fabricated PDMS stamps, and conducted microcontact printing to pattern single cardiomyocytes on the SMPs. Cardiomyocytes showed good confinement within the patterns before and after the application of dynamic mechanical stress.

Summary of Research:

Introduction. SMPs are smart materials that can undergo dynamic shape change stimulated by elevated temperature when they are programmed with internal strain [1]. Microcontact patterning is an efficient tool of controlling the shape of various cell types from tissue to single-cell level to study how the geometry confinement affects the cellular activities [2]. The combination of SMPs and microcontact patterning provides a platform for investigating remodeling of single cardiomyocytes to dynamic change of their geometry.

In this report, we focus on what we have achieved by microcontact patterning facilitated with CNF tools, which include a few steps: 1) design of a photomask with desired pattern shapes, 2) fabrication of Si wafers with opposite patterns by photolithography, 3) cure polydimethylsiloxane (PDMS) on top of wafers to make stamps and coat them with ECM proteins, 4) deposit ECM proteins through direct contact between stamps and SMPs, and 5) cell seeding on top of SMPs.

During this process, photomasks with patterns at high resolution and the efficient pattern transfer from masks to wafers ensure the perfect match of patterns between initial designs and final shapes.

Experimental Process. After estimating the areas of single cardiomyocytes, we designed rectangular and square patterns (areas: $1000 \mu\text{m}^2$ and $2000 \mu\text{m}^2$, aspect ratios: 1:1 and 1:3) with L-Edit software. Laser writing of photomasks was conducted by Heidelberg mask writer (DWL2000). After chrome etching and series washing steps, photomasks were ready to use. SU-8 50 photoresist was coated on top of a pre-cleaned Si wafer evenly with a photoresist spinner (spreading cycle: 500 rpm at 100 rpm per second for five seconds, spin cycle: 2000 rpm at 300 rpm per second for 30 seconds) to obtain a thickness of about $25 \mu\text{m}$. After prebaking at 65°C for three minutes and soft baking at 95°C for seven minutes, the wafer was cooled down to room temperature on a flat surface.

Before exposure, light source with wavelength below 365 nm was filtered out to avoid overexposure of top portion of resist film. After switching on the ABM contact aligner, the photomask was vacuumed on the raised mask frame, and the wafer was vacuumed on the substrate chuck. The mask and wafer were brought into contact by adjusting the position of substrate chuck. After setting exposure timer, the light source was moved on top of the mask to crosslink SU-8.

To test the accurate exposure time for getting optimal patterns, different regions of the wafer were exposed for various time periods. Exposed wafers were post baked at 65°C for one minute and then 95°C for three minutes. Patterns on wafers should be visible after seconds of post bake. After cooled down, wafers were immersed and agitated in SU-8 developer for four minutes to wash off un-crosslinked SU-8. Developed wafers were rinsed with isopropyl alcohol (IPA) and dried with nitrogen. The quality of patterns on wafers was checked under microscope, and optimal patterns should exhibit strong adhesion to the Si substrate and same dimensions as initial designs.

PDMS was cured on top of wafers at 60°C overnight and then cut into small stamps with similar sizes to SMP samples. 20 μ L of fluorescence-tagged fibronectin (100 μ g per mL) was pipetted on PDMS stamps and incubated at 37°C for one hour. After transfer to an environmental control room with 50% humidity, the fibronectin residual on the stamp was wicked off with KimWipe. Then the SMP was pressed on top of the stamp with a 20 g weight for two minutes to allow fibronectin transfer from the stamp to the SMP. After blocking with 0.4 % Pluronic F-127, single cardiomyocytes were seeded on SMPs at 5×10^4 cells per milliliter. After cultured at 28°C for two days, the patterned cells were transferred to 37°C for 24 hours, and the elevated temperature triggered the shape change of patterns (Figures 1, 2).

Patterned single cardiomyocytes transformed from square to elongated shape (Figures 3, 4).

Conclusion and Future Work:

In summary, we have fabricated Si wafers with single-cell scale patterns at CNF. We made PDMS stamps, and achieved efficient ECM protein transfer to SMPs through microcontact patterning.

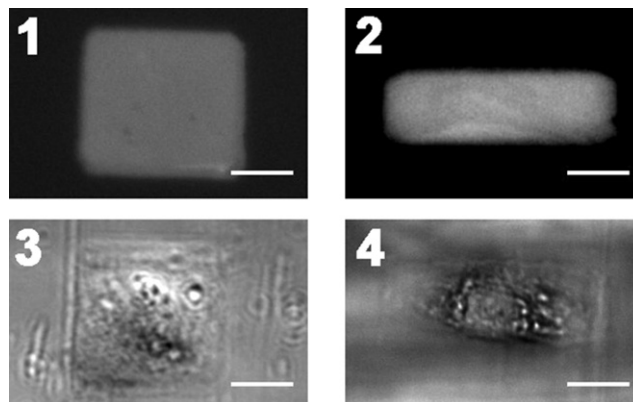


Figure 1: Fibronectin pattern on SMPs before shape change. Scale bar: 20 μ m. **Figure 2:** Fibronectin pattern on SMPs after shape change. Scale bar: 20 μ m. **Figure 3:** Patterned single cardiomyocyte on SMPs before shape change. Scale bar: 20 μ m. **Figure 4:** Patterned single cardiomyocyte on SMPs after shape change. Scale bar: 20 μ m.

We tested initial seeding of single cardiomyocytes on SMPs, and confirmed that they were elongated after triggering the shape change of SMPs. In future, we will run more cell seeding on our dynamic system to test the consistency of cell remodeling. The sarcomere organization and contractile functions will be quantified as evaluations of cellular responses.

References:

- [1] Davis, K. A., Burke, K. A., Mather, P. T. and Henderson, J. H. Dynamic cell behavior on shape memory polymer substrates. *Biomaterials* 32, 2285-2293 (2011).
- [2] Salick, M. R., et al. Micropattern width dependent sarcomere development in human ESC-derived cardiomyocytes. *Biomaterials* 35, 4454-4464 (2014).

Quantification of Recombinant Outer Membrane Vesicles for Vaccine

CNF Project Number: 2833-19

Principal Investigator(s): David Putnam

User(s): Mariela Rivera-De Jesús

Affiliation(s): Biomedical Engineering, Cornell University

Primary Source(s) of Research Funding: National Institutes of Health (R01AI139664), "Co-Presentation and Delivery of TLR Agonist Combinations with Subunit Antigens to Pathogen-Match the Immune Response" (E888866)

Contact: dap43@cornell.edu, mar524@cornell.edu

Primary CNF Tools Used: Malvern NS300 NanoSight

Abstract:

Bacteria-produced outer membrane vesicles (OMVs) are of great interest in the development of subunit vaccines. One challenge in their use as a vaccine platform is the difficulty of precisely quantifying OMVs. By using nanoparticle tracking analysis system, we can directly quantify the amount of recombinant OMVs produced and better adapt them for further applications. Recombinant ClearColi OMVs were indirectly quantified using bicinchoninic acid (BCA) assay and directly quantified using the Malvern NS300 NanoSight system, at different concentrations determined through the BCA assay. While no correlation was established between BCA-determined protein concentration and NTA-determined particle concentration, we have established a protocol for a direct quantification method of OMVs.

Summary of Research:

Outer membrane vesicles (OMVs) are 20 to 200 nm lipid nanoparticles produced by Gram negative bacteria. These vesicles contain the same surface proteins and sugars that are on the bacterial surface and are strong immunomodulators, an ability that has highlighted OMVs as a potential vaccine platform [1]. Bacteria can be recombinantly modified to produce OMVs with desired characteristics such as reduced toxicity and displaying of surface proteins. Our team is using recombinant bacteria to design a versatile OMV vaccine and investigate the co-presentation of antigens on OMVs. Indirect methods are the most employed, such as quantifying the total protein concentration or the dry mass of the vesicles, but it is important to have a precise measurement of the components of vaccines to produce reproducible results. One method for directly quantifying OMVs is through nanoparticle tracking analysis (NTA), using systems such as NanoSight [2].

Our goal is to develop a more precise method for measuring OMV concentration through NTA. In addition, if possible, we would like to establish a correlation between indirect quantification methods and NTA quantification methods.

Our group had previously modified ClearColi® (CC) BL21(DE3) cells to hypervesiculate through gene knockouts [3]. Three batches of CC OMVs were produced. In brief, liquid CC cultures were centrifuged (4°C, 15 min, 5,000 rcf) and the supernatant passed through a 0.2-mm filter.

The filtrate was ultracentrifuged (4°C, 3 hr, 26,000 rpm) and decanted, and the pellets resuspended in PBS. The protein concentration of each batch was determined using the Pierce™ Bicinchoninic Acid (BCA) Protein Assay Kit. Batches were then diluted to 1.50, 1.00, 0.75, 0.50, 0.25, and 0.10 ng/μL according to the BCA assay. Each dilution of each batch was finally measured using the Malvern NS300 NanoSight (five replicates, 1 min each) to determine particle concentration.

Conclusions and Future Steps:

Figure 1 compares the protein concentration measured using the BCA assay and the particle concentration using the NanoSight. Each slope was significantly different from each other, as further highlighted by Figure 2.

Further study is needed to establish a potential correlation between BCA and NTA quantification. Nonetheless, a successful method for measuring OMV concentration through NTA was established. While indirect quantification is enough for in-lab samples, NTA quantification can be applied to sample where a more precise quantification is required, such as determining vaccine dosing.

References:

- [1] Jan, AT. *Front Microbiol.* 2017; 8: 1-11.
- [2] Gerritzen, MJH, et al. *J. Extracell.* 2017; 19(8): 271.
- [3] Valentine, JL, et al. *Cell Chem Biol.* 2016; 23(6): 655-665.

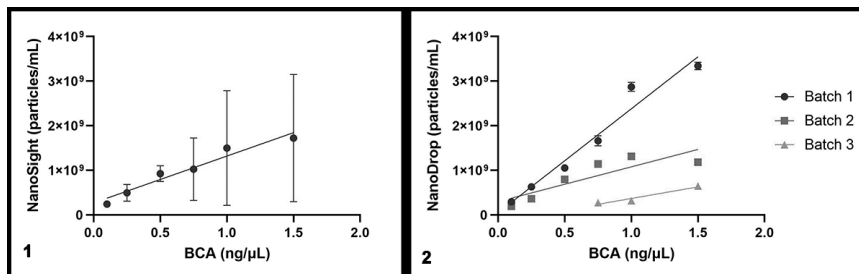


Figure 1, left: Comparison between BCA concentration and NanoSight concentration of CC OMVs, in individual batches. STD calculated by NanoSight. In Batch 3, the concentration of OMVs was too low to be measured below 0.75 ng/μL.

Figure 2, right: Comparison between BCA concentration and NanoSight concentration of CC OMVs, between all batches.